nature genetics

ARTICLES

https://doi.org/10.1038/s41588-020-00731-9

Check for updates

Interferons and viruses induce a novel truncated ACE2 isoform and not the full-length SARS-CoV-2 receptor

Olusegun O. Onabajo[1,8], A. Rouf Banday[1,8], Megan L. Stanifer[2], Wusheng Yan[1], Adeola Obajemu[1], Deanna M. Santer[3], Oscar Florez-Vargas[1], Helen Piontkivska[4], Joselin M. Vargas[1], Timothy J. Ring[1], Carmon Kee[5,6], Patricio Doldan[5,6], D. Lorne Tyrrell[3], Juan L. Mendoza[7], Steeve Boulant[5,6] and Ludmila Prokunina-Olsson[1]✉

Severe acute respiratory syndrome coronavirus 2 (SARS-CoV-2), which causes COVID-19, utilizes angiotensin-converting enzyme 2 (ACE2) for entry into target cells. *ACE2* has been proposed as an interferon-stimulated gene (ISG). Thus, interferon-induced variability in *ACE2* expression levels could be important for susceptibility to COVID-19 or its outcomes. Here, we report the discovery of a novel, transcriptionally independent truncated isoform of *ACE2*, which we designate as *deltaACE2* (*dACE2*). We demonstrate that *dACE2*, but not *ACE2*, is an ISG. In The Cancer Genome Atlas, the expression of *dACE2* was enriched in squamous tumors of the respiratory, gastrointestinal and urogenital tracts. In vitro, dACE2, which lacks 356 amino-terminal amino acids, was non-functional in binding the SARS-CoV-2 spike protein and as a carboxypeptidase. Our results suggest that the ISG-type induction of *dACE2* in IFN-high conditions created by treatments, an inflammatory tumor microenvironment or viral co-infections is unlikely to increase the cellular entry of SARS-CoV-2 and promote infection.

Cells expressing *ACE2* are potential targets of SARS-CoV-2 infection[1,2]. Studies based on single-cell RNA sequencing (scRNA-seq) of lung cells have identified type II pneumocytes, ciliated cells and transient secretory cells as the main types of *ACE2*-expressing cell[3,4]. Furthermore, *ACE2* was proposed to be an ISG, on the basis of its inducible expression in cells treated with interferons (IFNs) or infected by viruses that induce IFN responses, such as influenza[4,5]. These findings implied that the induction of *ACE2* expression in IFN-high conditions could result in an amplified risk of SARS-CoV-2 infection[4,5]. Concerns could also be raised about possible *ACE2*-inducing side effects of IFN-based treatments proposed for COVID-19 (refs. [6–9]).

ACE2 plays multiple roles in normal physiological conditions and as part of the host tissue-protective machinery in damaging conditions, including viral infections. As a terminal carboxypeptidase, ACE2 cleaves a single carboxy-terminal residue from peptide hormones such as angiotensin II and des-Arg9-bradykinin. ACE and ACE2 belong to the renin–angiotensin–aldosterone system, which regulates blood pressure and fluid–electrolyte balance; dysfunction of this system contributes to comorbidities in COVID-19 (refs. [10,11]). des-Arg9-bradykinin is generated from bradykinin and belongs to the kallikrein–kinin system, which is critical in regulating vascular leakage and pulmonary edema, early signs of severe COVID-19 (refs. [12,13]).

High plasma angiotensin II levels were found to be responsible for coronavirus-associated acute respiratory distress syndrome (ARDS), lung damage and high mortality in mouse models[14,15] and as a predictor of lethality in avian influenza in humans[16,17]. In the same conditions, ACE2, which decreases the levels of angiotensin II, was identified as a protective factor. The hijacking of the normal host tissue-protective machinery guarded by ACE2 was suggested as a mechanism through which SARS-CoV-2 could infect more cells[4,5]. Thus, it is critically important to identify factors affecting ACE2 expression in normal physiological processes and during viral infections and associated pathologies, such as in COVID-19.

Herein, aiming to explore the IFN-inducible expression of *ACE2* and its role in SARS-CoV-2 infection, we identified a novel, truncated isoform of *ACE2*, which we designate as *dACE2*. We then showed that *dACE2*, but not *ACE2*, is induced in various human cell types by IFNs and viruses; this information is important to consider for future therapeutic strategies and understanding COVID-19 susceptibility and outcomes.

Results

***dACE2* is a novel inducible isoform of *ACE2*.** To address the extent to which IFNs induce the expression of *ACE2* in human cells, we used our existing RNA-seq dataset (NCBI Sequence Read Archive (SRA): PRJNA512015) of a breast cancer cell line T47D infected with Sendai virus (SeV), known to be a strong inducer of IFNs and ISGs[18–20]. IFNs were not expressed in T47D cells at baseline, but SeV strongly induced expression of *IFNB1*, a type I IFN, and all type III

[1]Laboratory of Translational Genomics, Division of Cancer Epidemiology and Genetics, National Cancer Institute, National Institutes of Health, Bethesda, MD, USA. [2]Department of Infectious Diseases, Molecular Virology, University Hospital Heidelberg, Heidelberg, Germany. [3]Li Ka Shing Institute of Virology and Department of Medical Microbiology and Immunology, University of Alberta, Edmonton, Alberta, Canada. [4]Department of Biological Sciences and Brain Health Research Institute, Kent State University, Kent, OH, USA. [5]Division of Cellular Polarity and Viral Infection, German Cancer Research Center (DKFZ), Heidelberg, Germany. [6]Department of Infectious Diseases, Virology, University Hospital Heidelberg, Heidelberg, Germany. [7]Pritzker School of Molecular Engineering and Department of Biochemistry and Molecular Biology, University of Chicago, Chicago, IL, USA. [8]These authors contributed equally: Olusegun O. Onabajo, A. Rouf Banday. ✉e-mail: prokuninal@mail.nih.gov

IFNs (*IFNL1*, *2*, *3* and *4*). Several well-known ISGs (*ISG15*, *MX1* and *IFIT1*) were moderately expressed at baseline but were strongly induced by SeV (Supplementary Table 1). *ACE2* was not expressed at baseline but was strongly induced by SeV, exclusively as an isoform initiated from a novel first exon in intron 9 of the full-length *ACE2* gene (Fig. 1a,b).

RNA-seq analysis in T47D and RT-4 cell lines (Fig. 1b) demonstrated that *ACE2* exists as two full-length transcripts initiated from two independent first exons, which we designated as Ex1a and Ex1b (the latter is shared between these transcripts). Additionally, an alternative transcript was initiated from the novel first exon in intron 9, which we designated as Ex1c (Fig. 1b). The combination of ENCODE chromatin modification marks (H3K4me1, H3K4me3 and H3K27ac) and a cluster of DNase I hypersensitivity sites (Fig. 1a) suggests that Ex1c, but not Ex1a and Ex1b, is located within a putative regulatory region that might affect gene expression.

The novel *ACE2* isoform is predicted to encode a protein of 459 amino acids (aa), including the first 10 aa encoded by Ex1c. Compared to the full-length ACE2 protein of 805 aa, the truncation eliminates 17 aa of the signal peptide and 339 aa of the N-terminal peptidase domain (Fig. 1c). We designate this novel isoform as *dACE2* (NCBI GenBank accession number MT505392). Analysis of 100 vertebrate species with genomic sequences available through the UCSC Genome Browser showed that the putative dACE2 protein could be encoded only in primates (Supplementary Fig. 1a). Comparison of human Ex1c and its proximal promoter in select species showed 96.7–99.6% of sequence identity in primates and 54.0–73.5% in non-primate mammals (Supplementary Fig. 1b). In primates, despite some differences on the messenger RNA level, there was strong conservation within the putative protein encoded by *dACE2*-Ex1c (Fig. 1d,e).

Several binding motifs for transcription factors relevant for IFN signaling were predicted within the promoter of *dACE2*-Ex1c (P3; Fig. 2a). In contrast, ISG-type motifs were not predicted in the promoters of *ACE2*-Ex1a (P1) and *ACE2*-Ex1b (P2; Fig. 2a). We evaluated the IFN-inducible activity of all three promoters (*ACE2*-P1, *ACE2*-P2 and *dACE2*-P3) by testing their ability to drive expression of the luciferase reporter (Fig. 2b). The reporter constructs were transiently transfected into HepG2 cells, in which the signaling of all IFNs has been reported. Only *dACE2*-P3 significantly induced luciferase expression in response to 6 h of treatment with IFN-β or IFN-γ (Fig. 2c). The deletion of the first 100 base pairs of the *dACE2*-P3 promoter resulted in the loss of luciferase activity, suggesting that the predicted ISG-type motifs in the proximal promoter are important for IFN-driven *dACE2* expression (Fig. 2c). The promoter of *IFIT1*, an ISG, was used as a positive control and, as expected, was strongly responsive to treatments with IFNs (Fig. 2d).

***dACE2* is induced by in vitro treatment with IFNs.** We confirmed the SeV-induced expression of the full-length *dACE2* by PCR with reverse transcription (RT–PCR; Fig. 3a,b) and verified the corresponding PCR products by Sanger sequencing. Using custom-designed assays, we explored *ACE2* and *dACE2* expression in multiple cell lines at baseline and after SeV infection (Fig. 3c and Supplementary Table 2a). In most cell lines tested, *dACE2* but not *ACE2* was strongly upregulated by SeV infection (Fig. 3b,c). To directly address whether IFN was responsible for the induced expression of *dACE2*, we performed expression analysis in primary normal human bronchial epithelial (NHBE) cells[21] and human intestinal (colon and ileum) organoid cultures[22]. In NHBE cells from five healthy donors, the baseline expression levels of *dACE2* and *ACE2* were comparable, but only *dACE2* was significantly induced by treatment with IFN-α or IFN-λ3 (Fig. 3d and Supplementary Table 2b). In contrast, *ACE2* was expressed at high levels already at baseline both in colon and ileum organoid cultures, while the expression of *dACE2* was very low. Treatments with IFN-β or a cocktail of IFN-λ1–3 significantly induced only expression of *dACE2* and not *ACE2* (Fig. 3e and Supplementary Table 2c). In both cell models, the expression pattern of *dACE2* was similar to that of the known ISGs—*MX1* (Fig. 3d and Supplementary Table 2b) and *IFIT1* (Fig. 3e and Supplementary Table 2c).

***dACE2* is induced in virally infected human respiratory cells.** To investigate whether *dACE2* expression is induced by RNA viruses, which are potent inducers of the IFN response, we de novo quantified the expression of *ACE2*-Ex1a, *ACE2*-Ex1b and the newly annotated *dACE2*-Ex1c in several public RNA-seq datasets of virally infected human respiratory epithelial cells. In an RNA-seq dataset of human nasal airway epithelial cells from patients with asthma ex vivo infected with respiratory rhinovirus strains RV-A16 and RV-C15 (NCBI SRA: PRJNA627860), both *ACE2* and *dACE2* were expressed (Fig. 4a). Compared to that in uninfected cells, *dACE2*-Ex1c expression was strongly induced by both viruses—by RV-A16 (2.58-fold) and RV-C15 (2.42-fold)—while expression of *ACE2*-Ex1b was moderately induced only by RV-C15 (1.13-fold; Fig. 4b). Only *dACE2* expression strongly correlated with multiple ISGs and IFNs (Fig. 4c). Similarly, in human lung explants infected with a seasonal influenza A/H3N2 strain (NCBI SRA: PRJNA557257), only *dACE2* was induced by infection, and its expression correlated with the levels of IFNs and ISGs (Fig. 4d,e).

It was reported that, in contrast to *ACE2* expression in human cells, *Ace2* was not induced in primary mouse tracheal basal cells in response to in vitro and in vivo IFN stimulation, and on in vivo viral infection[4]. To explore this further, we analyzed a dataset for human and mouse lung cells infected with the respiratory syncytial virus (NCBI SRA: PRJNA588982). Indeed, we did not observe induction of *Ace2* in mouse lung cells (Extended Data Fig. 1a), while *dACE2* but not *ACE2* was induced in a human pulmonary carcinoma cell line (H292) infected with the respiratory syncytial virus (Extended Data Fig. 1b). These results illustrate that the identification of *ACE2* as an ISG[4,5] was likely based on the detection of inducible expression of *dACE2*, since 3'-scRNA-seq would detect both *ACE2* and *dACE2*. The differences between the human and mouse sequences corresponding to *dACE2*-Ex1c and promoters (Supplementary Fig. 1b) might be responsible for the lack of ISG-type *ACE2* expression in mice (Extended Data Fig. 1a). We also analyzed *Ace2* expression in an RNA-seq dataset of nasal washes from mock/SARS-CoV-2-infected ferrets and did not observe any *dAce2*-type transcripts (Extended Data Fig. 1c).

We also tested *ACE2* and *dACE2* expression in a commonly used cell line, Vero E6, derived from green monkey kidney. *ACE2* expression was high at baseline but not inducible by treatments with IFN-β or IFN-λ1 (which induced an ISG control, *MX1*), while *dACE2* was not detected in any conditions (Supplementary Table 2b). In comparison, in the human kidney cells HEK293T, *ACE2* expression was also high at baseline and not inducible by IFN treatment, while *dACE2* was moderately induced by IFN-β (Supplementary Table 2b). Although *dACE2* was not inducible by IFNs in Vero E6, while being moderately expressed in HEK293T cells, this should be further tested in additional cell lines and primary tissues before making conclusions about whether *dACE2* could be induced in non-human primates.

***dACE2* is enriched in squamous epithelial tumors.** We explored the expression patterns of *dACE2* in various human tissues. In a dataset of 95 normal human tissues of 27 types, *dACE2*-Ex1c was detectable in select tissues but at very low levels (≤10 RNA-seq reads), while *ACE2*-Ex1b expression was common (Extended Data Fig. 2). In the set of normal human tissues from the Genotype-Tissue Expression (GTEx) project, only total gene expression was available for *ACE2*, with the highest expression observed in the testes

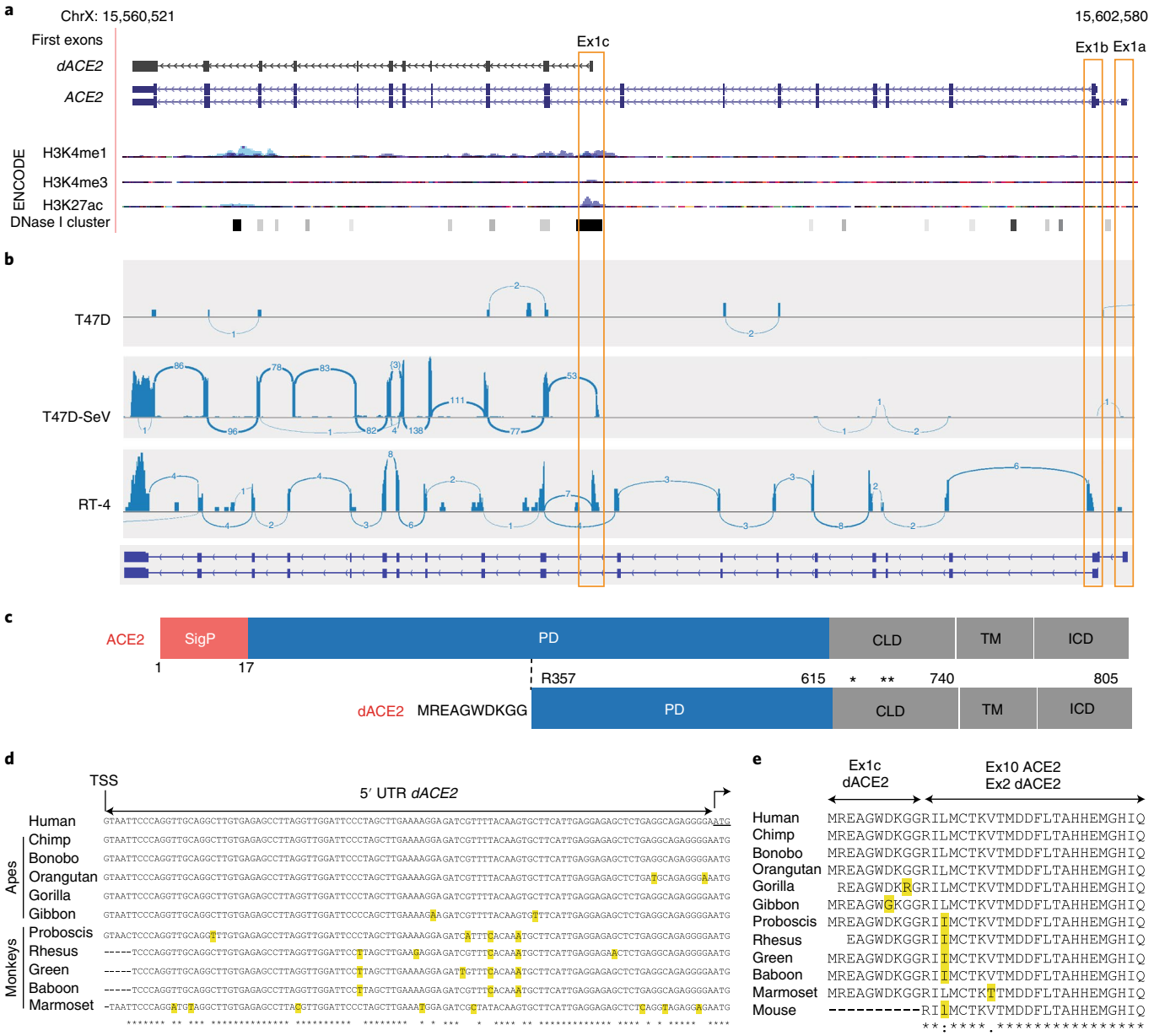

Fig. 1 | *dACE2* is a novel truncated virally induced isoform of *ACE2*. **a**, A UCSC Genome Browser view of the human *ACE2* region (chrX: 15,560,521–15,602,580, GRCh38/hg38) showing alternative first exons *ACE2*-Ex1a, *ACE2*-Ex1b and Ex1c, a novel first exon that creates a truncated *ACE2* isoform designated as *dACE2*. The combination of various ENCODE epigenetic marks for human cells, with H3K4me1, H3K4me3 and H3K27ac shown as peaks, and a cluster of DNase I hypersensitivity sites shown as bars indicates that *dACE2*-Ex1c is located within a putative regulatory region that can affect gene expression. The DNase I hypersensitivity site overlying Ex1c is detected in 38 of 95 cell lines tested. **b**, RNA-seq Sashimi plots depicting splicing patterns defining *ACE2* and *dACE2* isoforms in SeV/mock-infected T47D cells and uninfected RT-4 cells. The numbers on the Sashimi plots indicate the counts of exon–exon splicing reads. **c**, ACE2 is a single-span transmembrane protein with a signal peptide (SigP) of 17 aa and four functional domains—peptidase domain (PD, aa 18–615), collectrin-like domain (CLD, aa 616–740), transmembrane domain (TM, aa 741–761) and intracellular domain (ICD, aa 762–805). In dACE2, the signal peptide is not predicted; the peptidase domain starts from aa R357; the first 356 aa are replaced by 10 aa of a unique protein sequence; * and ** mark cleavage sites of the membrane-bound proteases ADAM17 and TMPRSS2, respectively. **d**,**e**, Sequence alignments of the 5′ UTR (**d**) and protein sequences encoded by *dACE2*-Ex1c and part of the downstream exon (**e**) in select primates. TSS, transcription start site. dACE2 is not predicted to be encoded in any non-primate species. Additional alignment analyses are shown in Supplementary Fig. 1a,b.

and small intestine (Supplementary Fig. 2). We hypothesized that as an ISG, *dACE2* might be absent or expressed at low levels in normal tissues, but could be induced by the inflammatory tissue microenvironment. We explored the data from The Cancer Genome Atlas (TCGA), which represents the largest collection of tumors and tumor-adjacent normal tissues, and de novo quantified the expression of *ACE2* and *dACE2* in all TCGA samples (Supplementary Table 2f–h). Expression of both *ACE2* and *dACE2* was detectable in many tumor-adjacent normal tissues (Fig. 5a and Extended Data Fig. 3). In the set of 10,185 TCGA tumors of 33 cancer types, *ACE2*-Ex1a, *ACE2*-Ex1b and *dACE2*-Ex1c were expressed in 12.6, 38.0 and 16.8% of tumors, respectively, with ≥5 RNA-seq reads per sample. *dACE2* was most expressed in head and neck squamous carcinoma (HNSC) and lung squamous

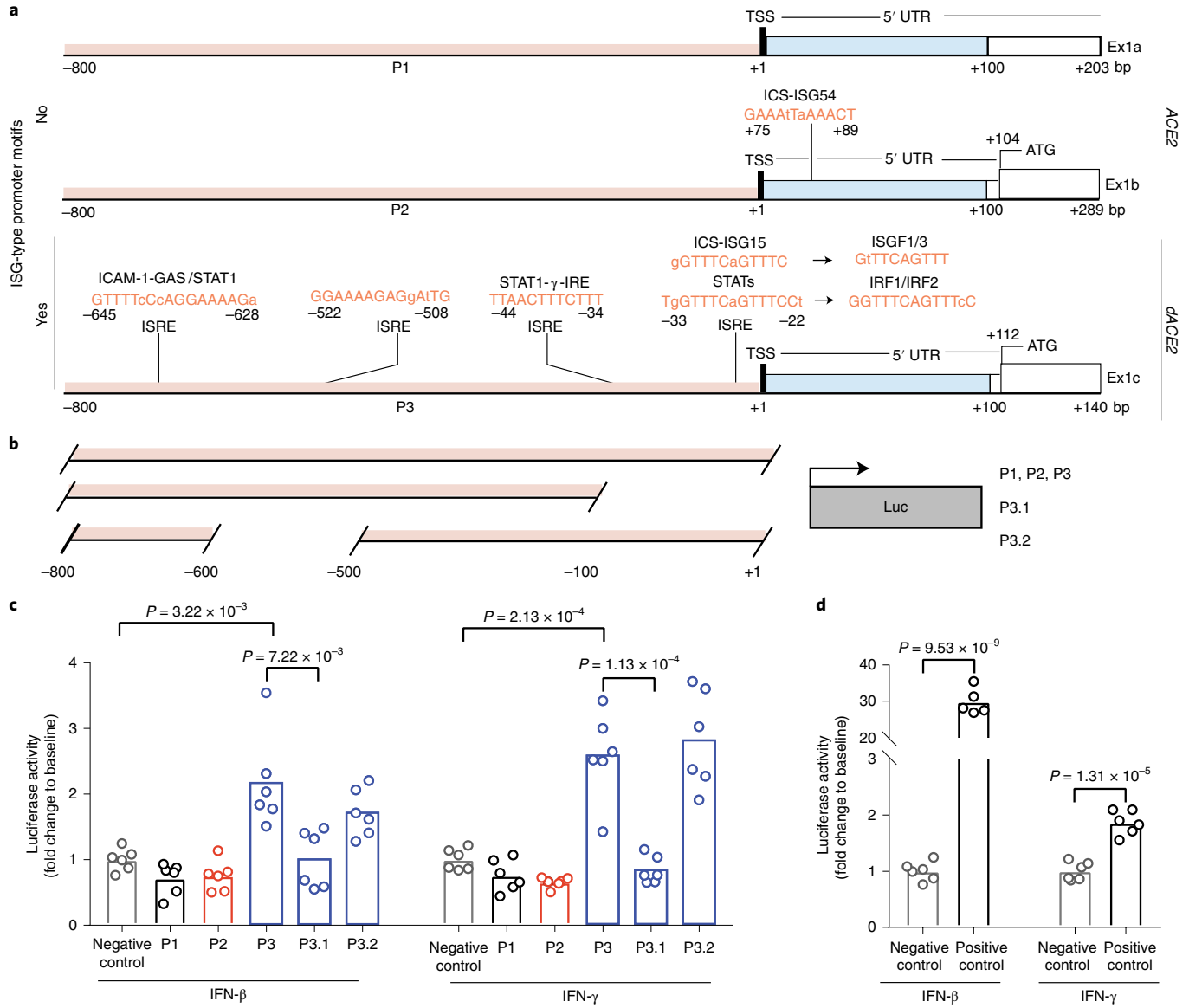

Fig. 2 | Evaluation of *ACE2* and *dACE2* promoters. a, Promoters of *ACE2* (P1 and P2) and *dACE2* (P3) were analyzed for binding motifs of transcription factors relevant for IFN signaling. Promoters were defined within the −800/+100 bp windows from the corresponding TSSs. ISRE, interferon-stimulated response element. **b**, Schematics of luciferase (Luc) reporter constructs. **c**, Luciferase activity in HepG2 cells transiently co-transfected with the indicated luciferase reporter constructs and *Renilla* (normalization control) and treated with 1 ng ml^{-1} of IFN-β or 2 ng ml^{-1} of IFN-γ for 6 h. **d**, Luciferase activity driven by the promoter of *IFIT1* (an ISG and positive control). Luciferase/*Renilla* ratios were normalized by corresponding mock-treated samples and are presented as fold change to the negative control (empty promoterless pGL4.21 vector). The *P* values are for unpaired, two-sided Student's *t*-tests. The experiment was conducted in six biological replicates per construct, and the results of one of three independent experiments are shown.

carcinoma (LUSC), which represent oral and bronchial mucosal epithelial surfaces, while *ACE2* was most expressed in kidney tumors (Extended Data Fig. 4).

Generally, *dACE2* expression was enriched in squamous tumors representing epithelial tracts. Squamous carcinomas of the lung (LUSC) and head and neck (HNSC) represent respiratory tract, esophageal cancer (ESCA)–upper gastrointestinal, and bladder cancer (BLCA) and cervical squamous carcinoma (CESC)–urogenital tract (Fig. 5a). In each tumor type, *dACE2* expression was significantly higher in squamous compared to non-squamous tumors and adjacent normal tissues (Fig. 5b). As tumors represent results of clonal expansion of individual cells, this analysis highlighted the differential etiology (squamous versus non-squamous) of *ACE2*- and *dACE2*-expressing cells in various tissues.

***dACE2* expression is IFN-γ inducible.** In addition to the cell-type origin, the observed enrichment of *dACE2* expression in some tumors might reflect persistent IFN exposure due to an inflammatory tumor microenvironment or underlying infection. An IFN-γ-induced signature emerged as a prominent feature in airway epithelial cells of patients with COVID-19, and this signature was linked with enrichment of cytotoxic T lymphocytes[5]. Unlike normal tissues, tumors are extensively infiltrated by immune cells, making the TCGA dataset particularly informative for the analysis of IFN signatures. *IFNG* was the most commonly expressed IFN gene in TCGA tumors (with 61% of all tumors expressing *IFNG* at RSEM ≥ 1, mean RSEM = 19.8), while other IFNs were expressed at low levels (mean RSEM ≤ 1.3; Extended Data Fig. 5a). *dACE2*-Ex1c levels significantly correlated ($P \leq 0.01$, $r \geq 0.2$) with

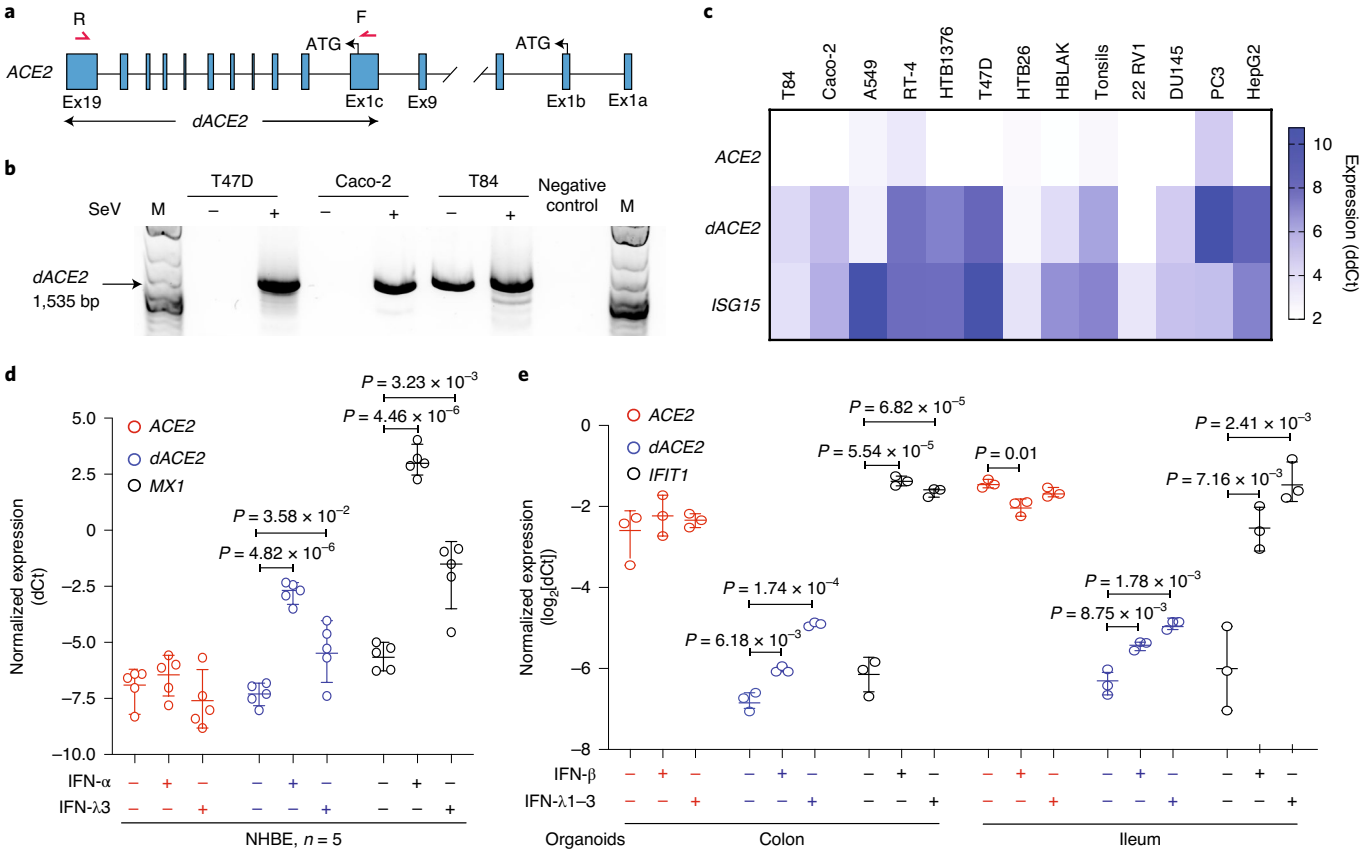

Fig. 3 | *dACE2* is induced by IFNs in vitro. a, A schematic representation of *ACE2* and *dACE2* transcripts and the positions of the forward (F) and reverse (R) PCR primers to generate full-length *dACE2* amplicons. **b**, An agarose gel showing an RT–PCR product of 1,535 bp corresponding to full-length *dACE2* in several cell lines with/without SeV infection. **c**, A heatmap of *ACE2* and *dACE2* expression and a positive control ISG (*ISG15*) measured by TaqMan expression assays in human cell lines infected with SeV for 12 h; the colors represent expression differences as ddCt normalized by endogenous controls (*GAPDH* and *ACTB*) and comparing SeV-infected to uninfected samples. **d**, The expression of *ACE2* and *dACE2* and a positive control ISG *MX1* in primary NHBE cells from five healthy donors; NHBEs were untreated or treated with IFN-α or IFN-λ3 for 24 h. The data are presented as means and s.d. The *P* values are for paired Student's *t*-tests. **e**, The expression of *ACE2*, *dACE2* and a positive control ISG *IFIT1* in colon and ileum organoid cultures from one donor; the organoids were treated with IFN-β or a cocktail of IFN-λ1–3 for 24 h in three biological replicates. The results are presented with means and s.d.; the *P* values are for unpaired, two-sided Student's *t*-tests. The full expression results are presented in Supplementary Table 2b,c.

IFNG expression in 8 out of 32 tumor types tested (Extended Data Fig. 5b), while *ACE2*-Ex1b showed only moderate and predominantly negative correlations with *IFNG* expression in some tumor types (Extended Data Fig. 5c). Furthermore, in vitro treatment with IFN-γ significantly induced *dACE2*, but not *ACE2* (Extended Data Fig. 5d). Thus, in addition to type I and type III IFNs (Fig. 3e–g), *dACE2* expression might be partly driven by IFN-γ contributed by tumor-infiltrating immune cells or inflamed virally infected tissues.

In the initial analysis of the TCGA-LUSC dataset ($n = 501$), which represents *ACE2*- and *dACE2*-expressing tumors of bronchial origin (Fig. 5b), *IFNG* expression did not correlate with *dACE2* (Extended Data Fig. 5b). To further investigate *ACE2* and *dACE2* expression in this tumor dataset, we used an unsupervised machine learning approach to assign all LUSC tumors to 6 clusters based on the expression of 270 ISGs[23] (Extended Data Fig. 6a,b). A set of ISGs ($n = 100$) that most strongly contributed to the definition of these clusters was used for correlation analysis. The analysis of a cluster that included 114 LUSC tumors with the highest ISG expression (cluster 5) showed that *dACE2* was strongly and significantly (false discovery rate (FDR) *P* value < 0.05) correlated with the expression of 20 ISGs and *ACE2*—with 5 ISGs (Extended Data Fig. 6c,d). Thus, ISG-type *dACE2* expression could be contributed by various factors, possibly determined by cell- and tissue-specific microenvironments and exposures.

***dACE2* is induced by SARS-CoV-2 in vitro.** Once we established that *dACE2* is an ISG in multiple human cell types under various conditions, we tested whether its expression could also be induced by SARS-CoV-2. There was a noticeable difference in the baseline expression levels of *ACE2* and *dACE2* in three cell lines tested (Calu3, Caco-2 and T84). Expression of *ACE2* and *dACE2* was much higher in the lung adenocarcinoma cell line Calu3 compared to both the colon adenocarcinoma cell lines Caco-2 and T84 (Fig. 6a and Supplementary Table 2d). The baseline *dACE2* expression in T84 was higher than in Caco-2, in line with the RT–PCR results (Fig. 1b). All cell lines were successfully infected with SARS-CoV-2 (Fig. 6b and Supplementary Table 2d), but *ACE2* expression was not affected by infection in any cell line tested (Fig. 6a and Supplementary Table 2d). Induction of *dACE2* expression tracked with previously reported SARS-CoV-2 infectivity rates in these cells[22]. Specifically, *dACE2* was most strongly induced in Caco-2 cells, in which over 80% of cells were infected by 24 h, moderately induced in T84 cells (20% of cells were infected) and not induced in Calu3 cells (10% of cells were infected). A similar expression pattern was observed for an ISG, *IFIT1*, except for in Calu3 cells, in which only *IFIT1* was significantly induced (Fig. 6a and Supplementary Table 2d). We performed similar analyses in human colon and ileum organoid cultures derived from three donors. Overall, the expression of

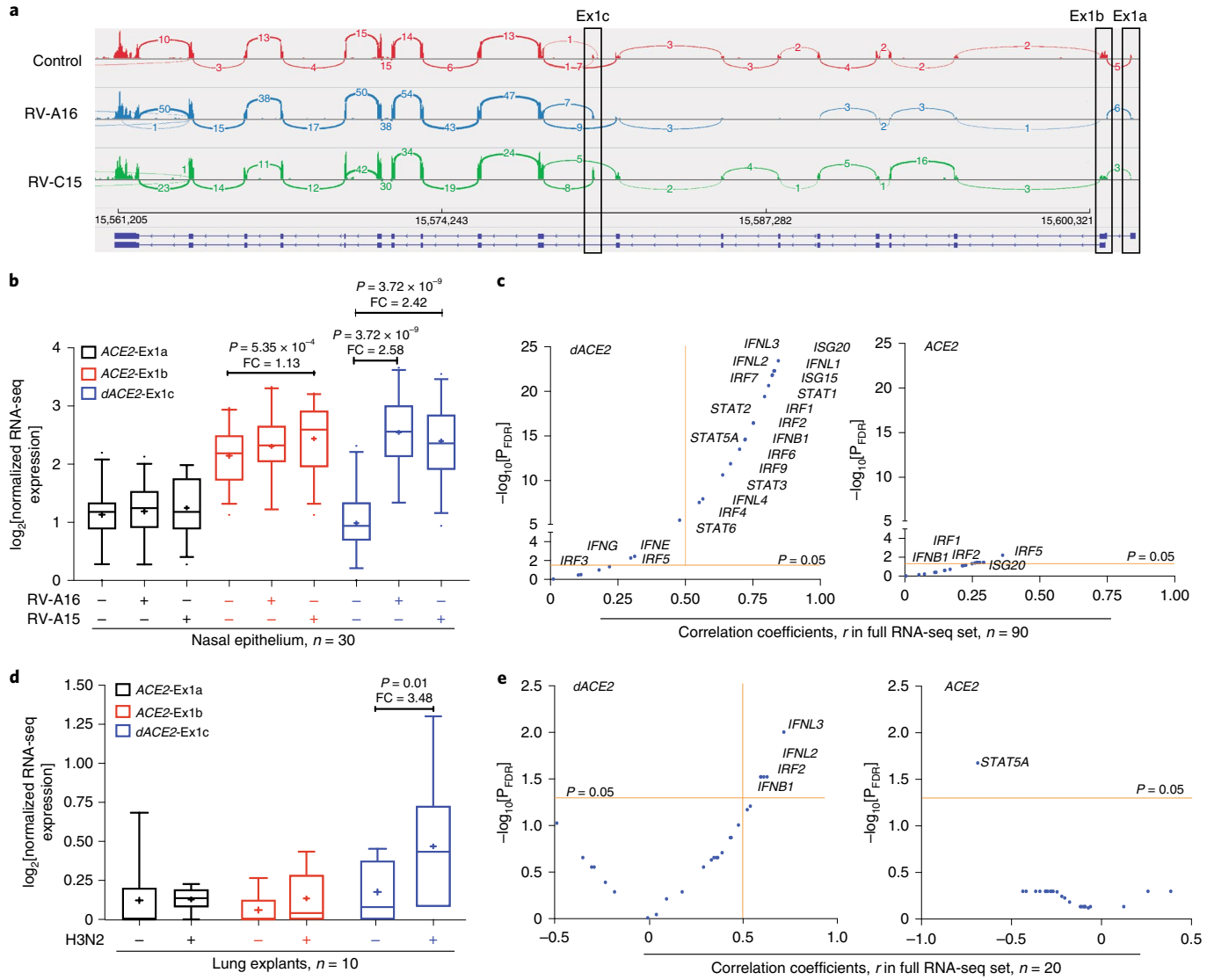

Fig. 4 | *dACE2* is induced in virally infected human respiratory cells. a–e, Expression patterns of *ACE2*, represented by Ex1a and Ex1b, and *dACE2*, represented by Ex1c, in uninfected and rhinovirus (RV)-infected human nasal epithelial cells (**a**–**c**) and in uninfected and influenza H3N2-infected cells from human lung explants (**d**,**e**). **a**, RNA-seq Sashimi plots. **b**,**d**, First-exon-specific expression levels of *ACE2* and *dACE2* are presented by box-and-whisker plots as: mean (+), median (center line), box (25th to 75th interquartile range), whiskers (5th–90th percentile range) and outliers (individual data points). FC, fold change compared to mock. The *P* values are for non-parametric, two-sided Wilcoxon matched-pairs signed rank tests. **c**,**e**, Pearson correlation coefficients with *P* values for two-sided tests for exon-specific expression levels of *ACE2* and *dACE2* with select ISGs and IFNs in the full datasets.

dACE2 and *IFIT1*, but not of *ACE2*, was significantly induced by SARS-CoV-2 infection (Fig. 6c,d and Supplementary Table 2e).

dACE2 is non-functional as a SARS-CoV-2 receptor and peptidase. Despite the strong induction of *dACE2* mRNA expression, we were unable to detect endogenous dACE2 in SeV-infected cell lines by western blotting with commercial antibodies for ACE2 (data not shown). However, in the proteome database of mass spectrometry data available for breast, colon and ovarian TCGA tumors[24], we detected human-specific peptides matching the 10 aa encoded by *dACE2*-Ex1c (Extended Data Fig. 7), suggesting that the dACE2 protein could be expressed in some conditions.

Transiently overexpressed dACE2–GFP was detected on the cell surface, although at levels lower than ACE2–GFP (Extended Data Fig. 8). However, the substantial N-terminal truncation by 356 aa in the peptidase domain of the putative dACE2 protein is expected to have important functional consequences compared to the activity of the full-length ACE2 protein of 805 aa. For example, decreased or no binding by the SARS-CoV-2 spike receptor-binding domain (RBD) would be expected for dACE2. Indeed, only cells overexpressing ACE2–GFP but not GFP alone or dACE2–Myc were able to bind and internalize the spike RBD (Fig. 7a–c). Compared to the case for ACE2–GFP alone, a moderately increased ACE2–GFP expression and binding of spike RBD was observed in cells co-expressing dACE2–Myc and ACE2–GFP (Fig. 7d,e and Extended Data Fig. 9a), which could suggest that dACE2 increases infection. However, when we transiently transfected ACE2–GFP with a plasmid for an unrelated transmembrane protein, TMEM129–Myc, we observed a similar pattern (Extended Data Fig. 9b,c). This suggests that the observed effect of dACE2 on the increased ACE2 levels and spike RBD binding might be a non-specific effect due to transient overexpression of multiple plasmids.

We then evaluated the effect of dACE2 expression on SARS-CoV-2 infection in the lung cancer cell line A549. The

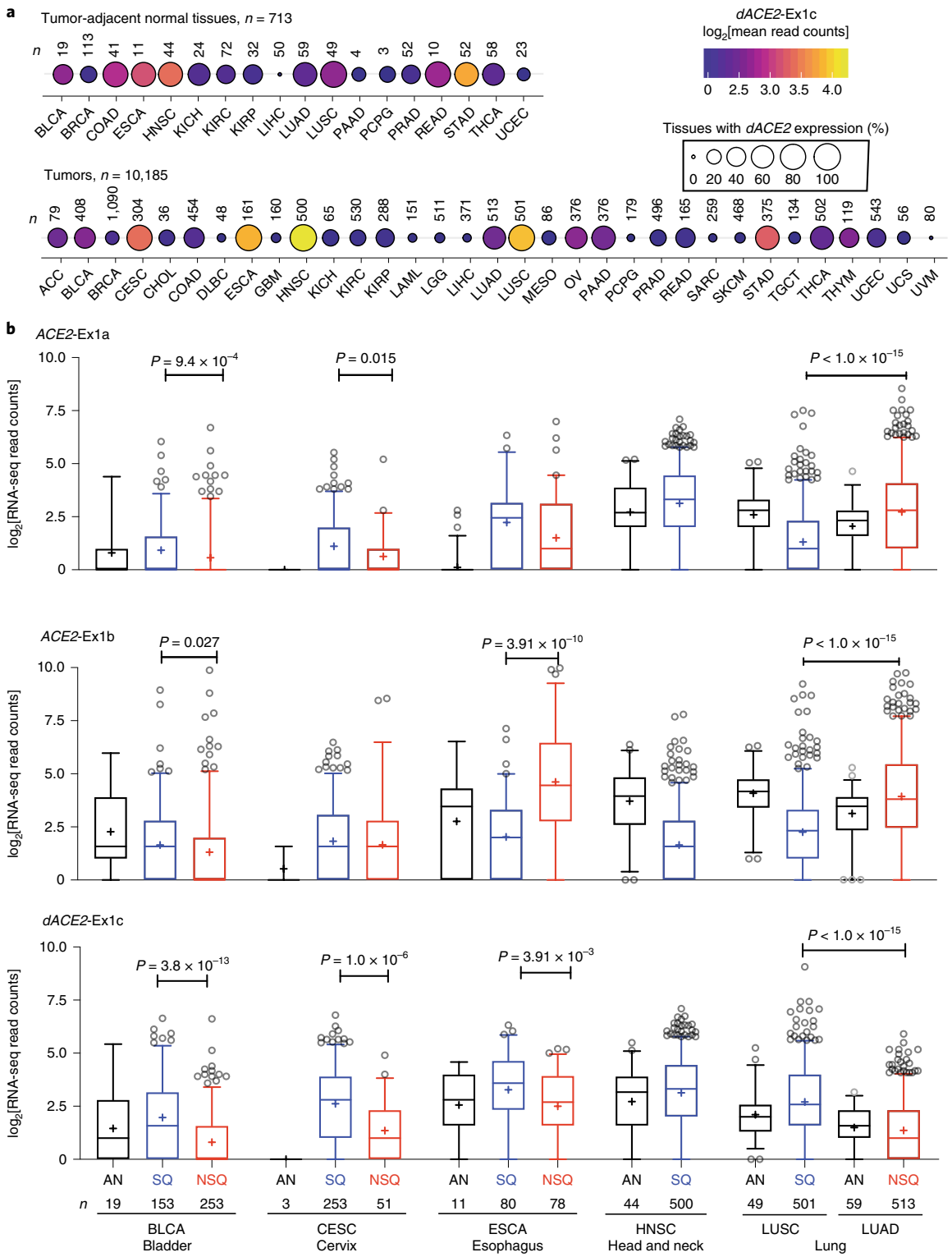

Fig. 5 | *dACE2* expression is enriched in squamous epithelial tumors. a, A bubble plot showing the mean expression levels (RNA-seq read counts) and proportions of samples with *dACE2*-Ex1c in TCGA tumor-adjacent normal tissues and 33 tumor types. d*ACE2*-Ex1c is expressed at relatively high levels and in many tumors of the bladder (BLCA), cervix (CESC), esophagus (ESCA), head and neck (HNSC) and lung squamous carcinoma (LUSC). **b**, RNA-seq counts of *ACE2*-Ex1a, *ACE2*-Ex1b and *dACE2*-Ex1c in tumor-adjacent normal tissues (AN), squamous tumors (SQ) and non-squamous tumors (NSQ). The *dACE2* expression is significantly higher in squamous compared to non-squamous tumors of the same tissue origin and corresponding tumor-adjacent normal tissues. Specifically, *dACE2*-Ex1c is expressed similarly in tumor-adjacent normal tissues adjacent to LUSC and lung adenocarcinoma (LUAD), while it is significantly higher in corresponding tumors and higher in LUSC than in LUAD, due to the clonal origin of these tumors from cells with differential expression of *dACE2*. The box-and-whisker plots represent mean (+), median (center line), box (25th–75th interquartile range), whiskers (5th–90th percentile range) and outliers (individual data points). The *P* values are for non-parametric, two-sided Mann–Whitney *U* tests.

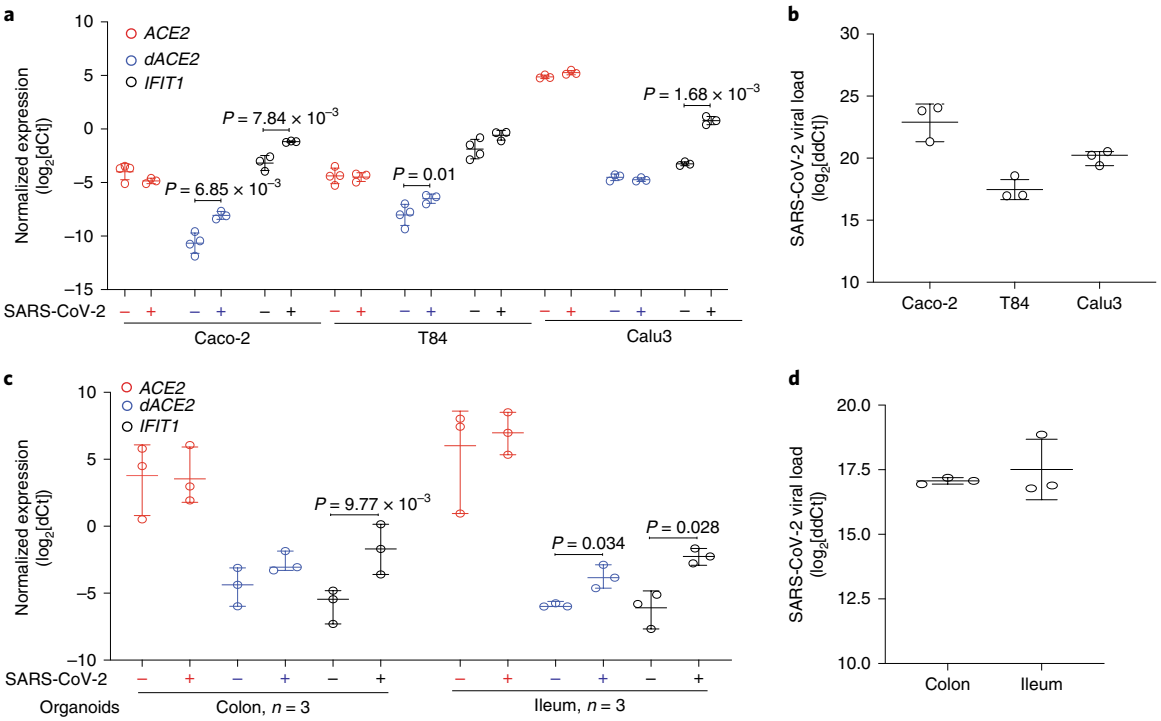

Fig. 6 | *dACE2* is induced by SARS-CoV-2 in human cell lines and organoid cultures. a–d, Expression of *ACE2*, *dACE2* and a control ISG *IFIT1* in the colon cancer cell lines Caco-2 and T84 and the lung cancer cell line Calu3 (all in three to four biological replicates) (**a**) and colon and ileum organoid cultures from three donors (**c**), and the SARS-CoV-2 viral loads in the corresponding cells (**b**,**d**). The *P* values are for two-sided Student's *t*-tests, unpaired tests for cell lines and paired tests for organoids. The results are presented with means and s.d.

wild-type A549 cells (transfected with GFP as a transient transfection control) were not infected by SARS-CoV-2, even after transfection with dACE2–Myc, because of low expression of endogenous *ACE2* (Extended Data Fig. 10a,b). However, the A549 cells stably expressing recombinant ACE2 (ACE2-stable) were infected (Fig. 7f,g and Extended Data Fig. 10c–h). These results further support the conclusion that, if expressed, dACE2 induced by viruses or IFNs is unlikely to increase SARS-CoV-2 infection.

The N-terminal truncation is also predicted to affect the carboxypeptidase activity of dACE2, which is important for its ability to cleave angiotensin II, des-Arg9-bradykinin and other substrates of ACE2. Indeed, we observed carboxypeptidase activity in lysates of cells transfected with ACE2–GFP but not with dACE2–GFP, and this activity was not affected by the addition of lysates of cells overexpressing dACE2–GFP (Fig. 7h,i).

Discussion

ACE2 was recently proposed to be an ISG because of its induction in IFN-high conditions, raising concerns about its potential role in increasing SARS-CoV-2 infection[4,5] and the safety of IFN-based treatments proposed for COVID-19. Our discovery of *dACE2*, a truncated version of *ACE2*, demonstrates that it is *dACE2* and not *ACE2* that is induced by IFNs and viruses, including SARS-CoV-2. Overexpressed recombinant dACE2, however, did not appear to bind SARS-CoV-2 spike RBD or affect the binding of ACE2 in our in vitro experiments, thus suggesting that ISG-type induction of *dACE2* would not increase viral entry.

Along with previously reported data[3,4], our results indicate that the expression of both *ACE2* and *dACE2* is limited to specific cell populations and conditions, contributing to low levels of their expression when analyzed by bulk RNA-seq methods. Although scRNA-seq analyses provide more specific information about cell populations that express these transcripts, the commonly used 3'-scRNA-seq methods do not discriminate between *ACE2* and *dACE2*. Thus, *dACE2* expression should be considered in expression studies of *ACE2* by various methods (RNA-seq, microarrays or targeted expression assays). By analyses in multiple human cell types and tissues, we showed that expression of *dACE2*, but not *ACE2*, is inducible by IFNs (type I, II and III) and viruses that induce IFN responses. Suppression of IFN signaling by SARS-CoV-2 has been reported by several studies[25,26], possibly explaining only a moderate effect of SARS-CoV-2 infection on *dACE2* induction in our experiments. While the levels and the role of type I and III IFNs in COVID-19 remain controversial[9,27–29], high levels of IFN-γ in the peripheral blood of patients with COVID-19 have been reported[5]. Thus, in tissues, *dACE2* could be induced owing to exposure to IFN-γ-expressing immune infiltrates[30–32]. Specifically, a 3'-scRNA-seq analysis showed *ACE2* induction by SARS-CoV-2 infection in ciliated epithelia, where high levels of IFN-γ-producing immune cells were also detected[5]. Our results strongly suggest that the induction of *dACE2* and not *ACE2* was detected in these patients.

We explored the extensive TCGA dataset of more than 10,000 tumors in which we de novo quantified *dACE2* expression based on RNA-seq data and concluded that IFN-γ-driven ISG signatures can be contributed by tumor-infiltrating immune cells. These conclusions can be extended to inflamed virally infected tissues, for which comparable RNA-seq data are limited by small sample sets, a low percentage of mappable reads due to substantially degraded input RNA, or unavailability of raw data due to patient privacy restrictions. Furthermore, the expression patterns observed in TCGA indicated that *dACE2* expression might be intrinsically enriched in squamous epithelial cells, which give rise to corresponding tumors of the respiratory, gastrointestinal and urogenital tracts. We found that in normal primary bronchial respiratory cells, the baseline expression levels of *dACE2* were comparable to

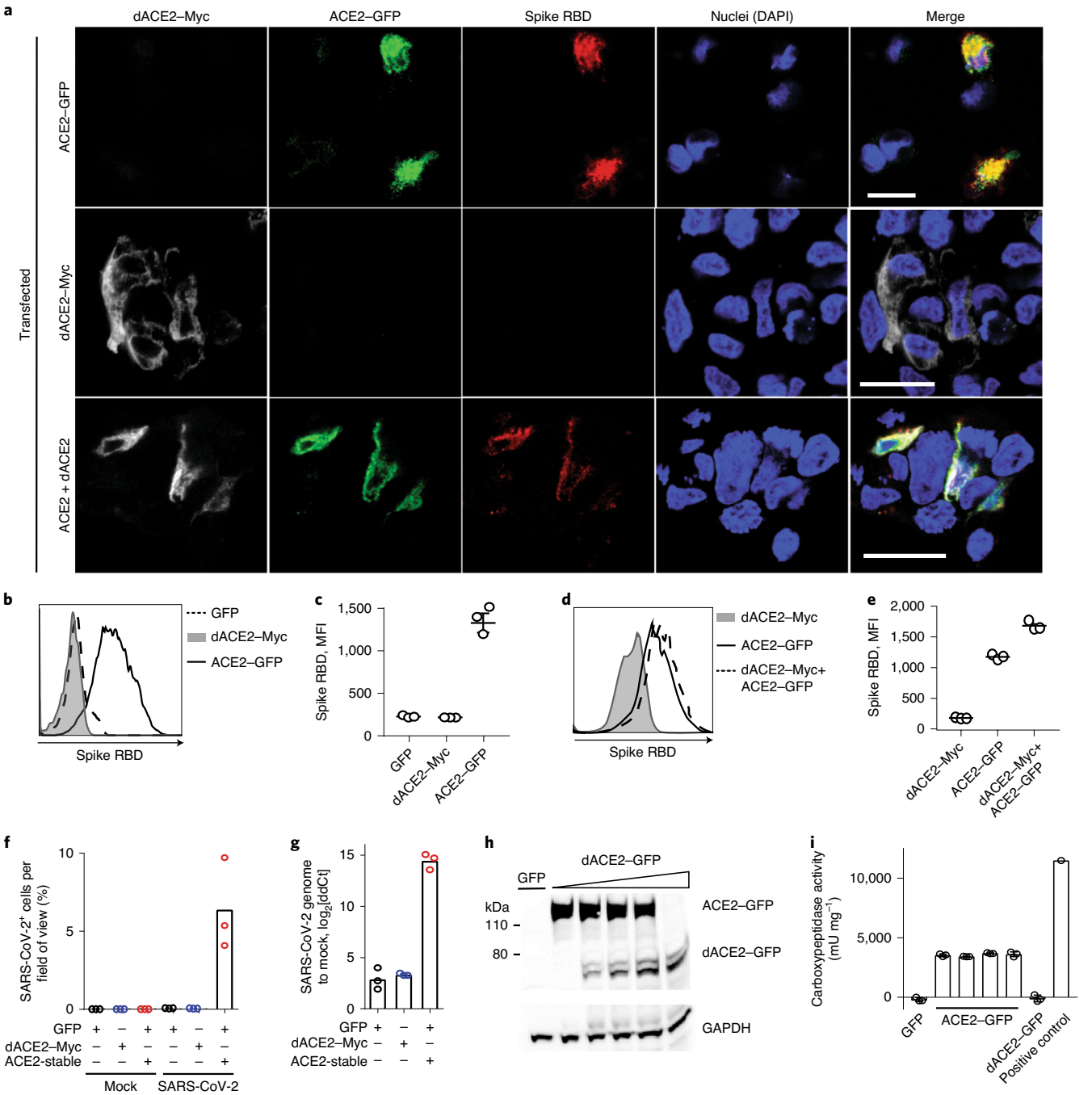

Fig. 7 | dACE2 is non-functional for binding SARS-CoV-2 spike protein RBD and as a carboxypeptidase. a, Representative confocal images of T24 cells transiently overexpressing dACE2–Myc (white) or ACE2–GFP (green) and treated with the RBD of the SARS-CoV-2 spike protein (red); nuclei (DAPI), blue. Scale bars, 20 μm. **b**–**e**, Representative flow cytometry histograms (**b**,**d**), and mean fluorescence intensity (MFI) values from three biological replicates (**c**,**e**), of spike RBD binding to the surface of ACE2–GFP- but not dACE2–Myc-expressing T24 cells. Gating for cells expressing dACE2–Myc, ACE2–GFP or both proteins is shown in Extended Data Fig. 9a. The results are based on three biological replicates, and represent one of two independent experiments. **f**, SARS-CoV-2 infectivity rates (%) in a lung cancer cell line, A549, transfected with GFP or dACE2–Myc, or stably expressing ACE2 (ACE2-stable) and transfected with GFP. **g**, The SARS-CoV-2 viral load as ddCt values compared to mock, corresponding to the plot in **f**. Additional details are provided in Extended Data Fig. 10. **h**, A representative western blot with an anti-ACE2 antibody that detects both recombinant ACE2–GFP and dACE2–GFP overexpressed in T24 cells. The amount of the ACE2–GFP lysate was kept constant, while the amount of the dACE2–GFP cell lysate was increased and the difference in the lysate volume was compensated by the empty GFP vector. **i**, The results of carboxypeptidase assays using variable amounts of lysates of cells (as described in the plot in **h**), showing that the activity of ACE2 is not affected by increasing amounts of dACE2. The results are based on three biological replicates and are presented with means and s.d. The western blot shows the results of one representative replicate.

those of *ACE2*, and further strongly induced by IFN treatments, suggesting some cell-type-specific role of *dACE2*, which should be further explored.

The detection of dACE2-specific peptides in some TCGA tumors and the predicted existence of dACE2 protein only in primates argue for its potentially important role. Although *dACE2*

expression was induced by IFNs and viruses in various human cell lines, dACE2 was not detected in these cell lines by western blotting with a C-terminal ACE2 antibody. The detection of endogenous dACE2 might require the generation of dACE2-specific antibodies. Alternatively, the translation of *dACE2* mRNA might be tightly regulated to exist only in specific conditions, as has been found for several mRNAs[33]. Further studies are required to confirm dACE2 cell surface expression in stable expression systems. However, on the basis of our in vitro data, we conclude that dACE2 does not increase the binding and cellular access of SARS-CoV-2 or serve as a carboxypeptidase. Extrapolation of these findings into biological and COVID-19-related mechanisms should be carried out with caution until confirmed by studies based on endogenous dACE2.

Although possible ISG-type ACE2 induction was considered as a risk for increasing SARS-CoV-2 infection, ACE2 deficiency rather than overexpression is discussed as a greater problem potentially contributing to COVID-19 morbidity[11–13,34]. Functional ACE2 deficiency occurs due to internalization of the SARS-CoV-2–ACE2 complex[2,35], which restricts ACE2 from performing its physiological functions, including its role as a carboxypeptidase for angiotensin II and des-Arg9-bradykinin and other peptide hormones. ACE2 deficiency might also be created owing to its regulation at the mRNA level, such as through regulation by microRNAs. The downregulation of ACE2 protein levels by miR-200c-3p has been reported in vitro[36]. Since miR-200c-3p binds to the 3′UTR shared by *ACE2* and *dACE2*, the ISG-type induction of *dACE2* might serve as a decoy for binding miR-200c-3p and possibly other microRNAs and reduce the downregulation of ACE2 protein. Expression of miR-200c-3p is induced through the NF-κB pathway during infection with the pandemic flu strain H5N1 and is associated with acute respiratory distress syndrome[36]. Signaling through the NF-κB pathway is hyper-activated by SARS-CoV infections[37], suggesting that miR-200c-3p could also be upregulated in patients with COVID-19, possibly resulting in decreased levels of ACE2 protein. In these conditions, the ISG-type induction of *dACE2* mRNA could be beneficial to preserve ACE2 protein levels. It will be important to examine this potential cross-talk between the ISG-type induction of *dACE2* and its role in the regulation of ACE2 protein levels, especially in COVID-19 conditions.

Patients with cancer are considered to be at a higher risk of more severe COVID-19 outcomes compared to the general population[38,39] owing to older age, comorbidities and the effects of cancer and cancer treatments. Patients with lung cancer are at a specifically increased risk of severe COVID-19 outcomes[38]. In our analysis, *dACE2* expression was common in tumors and particularly enriched in lung tumors of bronchial origin (LUSC), where the proper function of ACE2 is essential for protection from virus-induced tissue damage. The possible role of *dACE2* expression in COVID-19 outcomes, specifically in patients with cancer, should be further explored. ACE inhibitors (ACEIs) and angiotensin-receptor blockers (ARBs) are widely used to control hypertension and treat heart disease and chronic kidney disease[10]. Some concerns were raised that ACEIs and ARBs could induce ACE2 expression, leading to increased SARS-CoV-2 infection and possibly accounting for COVID-19 severity and high mortality in those who are likely to use these medications—older people and patients with cardiovascular disease. We demonstrated that *ACE2* expression is not inducible by IFNs, but it would be important to explore the effects of ACEIs and ARBs on *dACE2* expression to properly assess this risk. The effects of other factors, such as smoking, on *ACE2* and *dACE2* expression should also be considered.

In conclusion, we report the discovery and functional annotation of *dACE2*, an IFN-inducible isoform of *ACE2*. The existence of two functionally distinct *ACE2* isoforms reconciles several biological properties previously attributed to ACE2, with *dACE2* being an ISG, and ACE2 acting as the SARS-CoV-2 entry receptor and carboxypeptidase, without being regulated by IFNs. While our understanding of the functional role of dACE2, a novel ISG, is still unfolding, we believe these insights will clarify our knowledge on ACE2 and provide new research leads in understanding COVID-19 susceptibility, mechanisms and outcomes.

Online content

Any methods, additional references, Nature Research reporting summaries, source data, extended data, supplementary information, acknowledgements, peer review information; details of author contributions and competing interests; and statements of data and code availability are available at https://doi.org/10.1038/s41588-020-00731-9.

Received: 22 July 2020; Accepted: 28 September 2020;
Published online: 19 October 2020

References

1. Hoffmann, M. et al. SARS-CoV-2 cell entry depends on ACE2 and TMPRSS2 and is blocked by a clinically proven protease inhibitor. *Cell* **181**, 271–280 (2020).
2. Li, W. et al. Angiotensin-converting enzyme 2 is a functional receptor for the SARS coronavirus. *Nature* **426**, 450–454 (2003).
3. Lukassen, S. et al. SARS-CoV-2 receptor ACE2 and TMPRSS2 are primarily expressed in bronchial transient secretory cells. *EMBO J.* **39**, e105114 (2020).
4. Ziegler, C. G. K. et al. SARS-CoV-2 receptor ACE2 is an interferon-stimulated gene in human airway epithelial cells and is detected in specific cell subsets across tissues. *Cell* **181**, 1016–1035 (2020).
5. Chua, R. L. et al. COVID-19 severity correlates with airway epithelium–immune cell interactions identified by single-cell analysis. *Nat. Biotechnol.* **38**, 970–979 (2020).
6. Zhou, Q. et al. Interferon-α2b treatment for COVID-19. *Front. Immunol.* **11**, 1061 (2020).
7. Hung, I. F. et al. Triple combination of interferon beta-1b, lopinavir-ritonavir, and ribavirin in the treatment of patients admitted to hospital with COVID-19: an open-label, randomised, phase 2 trial. *Lancet* **395**, 1695–1704 (2020).
8. Prokunina-Olsson, L. et al. COVID-19 and emerging viral infections: the case for interferon lambda. *J. Exp. Med.* **217** (2020).
9. O'Brien, T. R. et al. Weak induction of interferon expression by SARS-CoV-2 supports clinical trials of interferon lambda to treat early COVID-19. *Clin. Infect. Dis.* **71**, 1410–1412 (2020).
10. Re, R. N. Mechanisms of disease: local renin-angiotensin-aldosterone systems and the pathogenesis and treatment of cardiovascular disease. *Nat. Clin. Pract. Cardiovasc. Med.* **1**, 42–47 (2004).
11. Diamond, B. The renin-angiotensin system: an integrated view of lung disease and coagulopathy in COVID-19 and therapeutic implications. *J. Exp. Med.* **217**, jem.20201000 (2020).
12. van de Veerdonk, F. L. et al. Kallikrein–kinin blockade in patients with COVID-19 to prevent acute respiratory distress syndrome. *eLife* **9**, e57555 (2020).
13. de Maat, S., de Mast, Q., Danser, A. H. J., van de Veerdonk, F. L. & Maas, C. Impaired breakdown of bradykinin and its metabolites as a possible cause for pulmonary edema in COVID-19 infection. *Semin. Thromb. Hemost.* https://doi.org/10.1055/s-0040-1712960 (2020).
14. Imai, Y. et al. Angiotensin-converting enzyme 2 protects from severe acute lung failure. *Nature* **436**, 112–116 (2005).
15. Kuba, K. et al. A crucial role of angiotensin converting enzyme 2 (ACE2) in SARS coronavirus-induced lung injury. *Nat. Med.* **11**, 875–879 (2005).
16. Huang, F. et al. Angiotensin II plasma levels are linked to disease severity and predict fatal outcomes in H7N9-infected patients. *Nat. Commun.* **5**, 3595 (2014).
17. Zou, Z. et al. Angiotensin-converting enzyme 2 protects from lethal avian influenza A H5N1 infections. *Nat. Commun.* **5**, 3594 (2014).
18. Middlebrooks, C. D. et al. Association of germline variants in the APOBEC3 region with cancer risk and enrichment with APOBEC-signature mutations in tumors. *Nat. Genet.* **48**, 1330–1338 (2016).
19. Obajemu, A. A. et al. IFN-lambda4 attenuates antiviral responses by enhancing negative regulation of IFN signaling. *J. Immunol.* **199**, 3808–3820 (2017).
20. Minas, T. Z. et al. *IFNL4*-ΔG is associated with prostate cancer among men at increased risk of sexually transmitted infections. *Commun. Biol.* **1**, 191 (2018).
21. Santer, D. M. et al. Differential expression of interferon-lambda receptor 1 splice variants determines the magnitude of the antiviral response induced by interferon-lambda 3 in human immune cells. *PLoS Pathog.* **16**, e1008515 (2020).

22. Stanifer, M. L. et al. Critical role of type III interferon in controlling SARS-CoV-2 infection in human intestinal epithelial cells. *Cell Rep.* **32**, 107863 (2020).
23. Schoggins, J. W. et al. A diverse range of gene products are effectors of the type I interferon antiviral response. *Nature* **472**, 481–485 (2011).
24. Wen, B., Wang, X. & Zhang, B. PepQuery enables fast, accurate, and convenient proteomic validation of novel genomic alterations. *Genome Res.* **29**, 485–493 (2019).
25. Blanco-Melo, D. et al. Imbalanced host response to SARS-CoV-2 drives development of COVID-19. *Cell* **181**, 1036–1045 (2020).
26. Chu, H. et al. Comparative replication and immune activation profiles of SARS-CoV-2 and SARS-CoV in human lungs: an ex vivo study with implications for the pathogenesis of COVID-19. *Clin. Infect. Dis.* **71**, 1400–1409 (2020).
27. Lee, J. S. et al. Immunophenotyping of COVID-19 and influenza highlights the role of type I interferons in development of severe COVID-19. *Sci. Immunol.* **5**, eabd.1554 (2020).
28. Broggi, A. et al. Type III interferons disrupt the lung epithelial barrier upon viral recognition. *Science* **369**, 706–712 (2020).
29. Major, J. et al. Type I and III interferons disrupt lung epithelial repair during recovery from viral infection. *Science* **369**, 712–717 (2020).
30. Lucas, C. et al. Longitudinal analyses reveal immunological misfiring in severe COVID-19. *Nature* **584**, 463–469 (2020).
31. Lagunas-Rangel, F. A. & Chavez-Valencia, V. High IL-6/IFN-gamma ratio could be associated with severe disease in COVID-19 patients. *J. Med. Virol.* **92**, jmv.25900 (2020).
32. Thijsen, S. et al. Elevated nucleoprotein-induced interferon-gamma release in COVID-19 patients detected in a SARS-CoV-2 enzyme-linked immunosorbent spot assay. *J. Infect.* **81**, 452–482 (2020).
33. Leppek, K., Das, R. & Barna, M. Functional 5' UTR mRNA structures in eukaryotic translation regulation and how to find them. *Nat. Rev. Mol. Cell Biol.* **19**, 158–174 (2018).
34. Zores, F. & Rebeaud, M. E. COVID and the renin–angiotensin system: are hypertension or its treatments deleterious? *Front. Cardiovasc. Med.* **7**, 71 (2020).
35. Wan, Y., Shang, J., Graham, R., Baric, R. S. & Li, F. Receptor recognition by the novel coronavirus from Wuhan: an analysis based on decade-long structural studies of SARS coronavirus. *J. Virol.* **94**, e00127-20 (2020).
36. Liu, Q. et al. miRNA-200c-3p is crucial in acute respiratory distress syndrome. *Cell Discov.* **3**, 17021 (2017).
37. Hirano, T. & Murakami, M. COVID-19: a new virus, but a familiar receptor and cytokine release syndrome. *Immunity* **52**, 731–733 (2020).
38. Mehta, V. et al. Case fatality rate of cancer patients with COVID-19 in a New York hospital system. *Cancer Discov.* **10**, 935–941 (2020).
39. Kuderer, N. M. et al. Clinical impact of COVID-19 on patients with cancer (CCC19): a cohort study. *Lancet* **395**, 1907–1918 (2020).

Methods

Cells. All cell lines and primary cells used are listed in Supplementary Table 3. Cell lines were either used within 6 months after purchase or were periodically authenticated by microsatellite fingerprinting (AmpFLSTR Identifiler, Thermo Fisher) by the Cancer Genomics Research Laboratory/NCI. All cell lines were regularly tested for mycoplasma contamination using the MycoAlert Mycoplasma Detection kit (Lonza). The previously described[21] NHBE cells were isolated from normal lungs that were not used for transplantation. The lungs were obtained from de-identified donors via a tissue retrieval service (International Institute for the Advancement of Medicine, Edison, NJ) with ethical approval from the Conjoint Health Research Ethics Board of the University of Calgary and the Internal Ethics Board of the International Institute for the Advancement of Medicine. Anonymized human tissue from colon resections was obtained from the University Hospital Heidelberg, in accordance with the recommendations of the University Hospital Heidelberg and written informed consent obtained from all participants in accordance with the Declaration of Helsinki. The protocol (S-443/2017) was approved by the Ethics Commission of the University Hospital Heidelberg. Organoids were generated from these tissues, as previously described[22].

Viral infections. Stocks of SeV Cantell strain were purchased from Charles River Laboratories. The cells listed in Supplementary Table 3 were infected in duplicates or triplicates with SeV (7.5×10^5 50% chicken embryo infectious dose per milliliter) for 12 h as previously described[18–20]. SARS-CoV-2 (strain BavPat1) was obtained from C. Drosten at the Charité in Berlin, Germany, and provided via the European Virology Archive.

Infections with SARS-CoV-2 were performed with a multiplicity of infection of 1 in cell lines and 3×10^5 focus-forming units of the virus in organoids on the basis of titers in Vero E6 cells. Infections in colon cancer cell lines (Caco-2 and T84), a lung cancer cell line (Calu3) and colon and ileum organoid cultures were previously described[22]. Lung cancer cells A549 (wild-type or stably overexpressing human ACE2 (ACE2-stable)) were seeded either in 48-well plates (for RNA) or on iBIDI glass-bottom 8-well chamber slides (for immunofluorescence analysis) at a density of 7.5×10^4 cells per well or chamber. Cells were transduced at 24 h post-seeding with lentiviruses expressing GFP or dACE2–Myc and infected 3 days post-transduction. Culture medium was removed and the virus was added to cells for 1 h at 37 °C. After virus removal, cells were washed 1× with PBS, and medium was added back to the cells. Cells were collected at 24 h post-infection for RNA extraction or were fixed in 4% paraformaldehyde for 20 min at room temperature for infectivity analysis by immunofluorescence staining, as was previously described[22]. Briefly, cells were washed and permeabilized in 0.5% Triton-X for 15 min at room temperature. A mouse monoclonal antibody against SARS-CoV-2 nucleoprotein (Sino Biologicals) was diluted in PBS and incubated for 1 h at room temperature. Cells were washed in 1× PBS three times and incubated with goat anti–mouse Alexa Fluor 568 (Molecular Probes) and DAPI for 45 min at room temperature. Cells were washed in 1× PBS three times and imaged by epifluorescence on a Nikon Eclipse Ti-S (Nikon) to quantify the number of infected cells relative to the number of nuclei. It was determined that infection rates were 80% in Caco-2 cells, ~20% in T84 cells and ~10% in Calu3 cells and organoids[22]. Organoids from three donors were infected in three or four biological replicates that were averaged and presented as one value per donor.

PCR, cloning and Sanger sequencing. Complementary DNA was synthesized from 250 ng of total RNA per 20 µl reaction using the RT² First Strand cDNA kit and random hexamers (Qiagen). PCR for the full-length *dACE2* was performed using the primers and conditions listed in Supplementary Table 4. PCR-amplified products were resolved on 1% agarose gel, cut, purified and Sanger-sequenced. After the cDNA sequences were validated, constructs for dACE2 with C-terminal Myc–DDK and GFP tags cloned in the pcDNA3.4 vector were custom-synthesized by Thermo Fisher. ACE2 with a C-terminal GFP tag (RG208442) and a Myc–DDK tag (RC208442) were purchased from Origene. The empty vectors pMax-GFP (Lonza) and pCMV6-AC-Myc-DDK (Origene) were used as controls.

Treatments with IFNs. All IFNs used are listed in Supplementary Table 5. IFN treatment of NHBE cells was previously described[21]. Briefly, cells were cultured in BEGM with supplements (Lonza), seeded in 6-well plates and utilized at ~70% confluency (typically after 10–11 days with a medium change every 2 days). Cells were left untreated or treated with IFN-α2b (INTRON A, Merck, 100 IU ml^{-1}) or IFN-λ3 (R&D Systems, 100 ng ml^{-1}) for 24 h. Cells were washed with PBS, resuspended in TRIzol (Thermo Fisher) and stored at −80 °C for future RNA isolation. IFN treatment of human colon and ileum organoids was previously described[22]. Briefly, at ~70% of cell confluence, the medium was replaced with a cocktail of IFN-λ1–3 (100 ng ml^{-1} of each for a total of 300 ng ml^{-1}) for 24 h. T84 and Caco-2 cells were treated with IFN-γ (2 ng ml^{-1}) for 24 h.

Quantitative RT–PCR. Total RNA was extracted using the RNAeasy kit (Qiagen) from all samples except for NHBEs, for which the Direct-zol mini RNA isolation kit was used (Zymo Research). cDNA was synthesized from the total RNA with the RT² First Strand kit (Qiagen, for all cell lines except for SARS-CoV-2-infected cells), Superscript VILO IV (Thermo Fisher, for NHBEs) or the iSCRIPT cDNA kit (Bio-Rad, for organoids and SARS-CoV-2-infected cell lines), always with an additional DNase I treatment step. Quantitative RT–PCR assays were performed in technical duplicates in 96- or 384-well plates on a QuantStudio 7 (Life Technologies) or Bio-Rad CFX 96 instrument, with RT² SYBR Green (Qiagen), POWER SYBR (Thermo Fisher), iTaq SYBR (Bio-Rad) or TaqMan (Thermo Fisher) expression assays (Supplementary Table 4). The expression of target genes was normalized by geometric means of endogenous controls (*GAPDH*, *HPRT1*, *TBP* or *ACTB*, as indicated in Supplementary Table 2a), and is presented as dCt values relative to endogenous controls ($\log_2$ scale). For cell lines, the analyses were based on biological replicates for samples obtained from donors (NHBEs and organoids), and 3–4 biological replicates were averaged and presented per donor.

RNA sequencing (RNA-seq) of T47D and RT-4 cells. Total RNA was extracted from T47D and RT-4 cells by using the RNeasy Mini kit with an on-column DNase digestion (Qiagen) and treated with Ribo-Zero (Illumina). RNA-seq libraries were prepared from high-quality RNA samples (RIN scores >9.0) with the KAPA Stranded RNA-seq kit with RiboErase (Roche). Paired 150-bp reads (21.2–118.8 million reads per sample) were generated with HiSeq 2500 (Illumina) by the Cancer Genomics Laboratory (Division of Cancer Epidemiology and Genetics, National Cancer Institute (DCEG/NCI)). The reads were aligned with STAR alignment tool version 7.1.2a (21) using the GRChg37/hg19 genome assembly and visualized using the Integrative Genomics Viewer. The RNA-seq dataset of a breast cancer cell line, T47D, infected with SeV was deposited as NCBI SRA: PRJNA512015.

RNA-seq analysis of data from NCBI SRA and TCGA. RNA-seq datasets (Supplementary Table 6) were downloaded from NCBI SRA using SRA tools. The FASTQ files were compressed using GZIP and aligned with STAR version 7.1.3a to the human GRChg38/hg38 genome assembly. BAM files with ≤80% of mappable reads were excluded. BAM files were indexed and sliced using SAMtools to include 51.6 kilobases of the human *ACE2* genomic region (chrX: 15,556,393–15,608,016, hg38). For non-human RNA-seq datasets, the alignment was performed with the reference genomes mm10 for mice, and MusPutFur1.0 for ferrets. For TCGA STAR-aligned RNA-seq data, BAM slices for the *ACE2* region were acquired for 10,898 TCGA samples (10,185 tumors and 713 tumor-adjacent normal tissues) through the NCI Genomics Data Commons portal accessed on 12 May 2020, using workflow https://docs.gdc.cancer.gov/API/Users_Guide/BAM_Slicing/.

Estimation of RNA-seq read counts for *ACE2* exons. RNA-seq reads corresponding to *ACE2*-Ex1a, *ACE2*-Ex1b and *dACE2*-Ex1c were counted by processing RNA-seq BAM slices using the R package ASpli version 1.5.1 with default settings. Genomic coordinates were manually curated in the GTF file and the 'counts' function was used to generate and export RNA-seq reads for the selected exons in a tab file format. The analysis of exon expression patterns within tissue subtypes was based on $\log_2$-transformed raw reads for each exon. The reads were normalized by dividing by the exon length (Supplementary Table 7) and multiplying by the geometric mean of the total reads of the three exons (Ex1a, Ex1b and Ex1c) across all samples as a scaling factor to adjust for variability in sequencing coverage between samples. Correlation analyses of $\log_2$[normalized exon expression + 1] of *ACE2*-Ex1a, *ACE2*-Ex1b and *dACE2*-Ex1c with $\log_2$[transcripts per million + 1] of IFNs, genes encoding signal transducers and activators of transcription (STATs), interferon regulatory factors (IRFs) and select ISG controls (*ISG15* and *ISG20*) were performed in R using the package dplyr.

Expression values for all *IFN* genes for all tumors in the TCGA PanCancer Atlas were downloaded as RSEM values from the cBioPortal for Cancer Genomics (https://www.cbioportal.org/). Expression of *IFNL4*, a most recently discovered IFN (ref. [40]), was not available in the TCGA dataset based on the hg19/GRCh37 reference. As *IFNG* was expressed in most samples compared to other IFN genes (Extended Data Fig. 5a), it was used for further analysis. Correlation analyses of the $\log_2$[normalized exon expression + 1] of *ACE2*-Ex1b and *dACE2*-Ex1c were performed with $\log_2$[RSEM + 1] values for *IFNG*. Correlation patterns between *IFNG* and *ACE2*-Ex1a were similar to those between *IFNG* and *ACE2*-Ex1b (data not shown). Correlation analyses were performed with Spearman and Pearson methods and provided similar results. The *P* values and coefficients presented are for Pearson correlations.

Unsupervised clustering and correlation analyses in TCGA. Gene expression *Z*-scores in the lung squamous cell carcinoma (TCGA-LUSC, $n=501$) dataset were calculated for 270 ISGs from a previously curated list[23]. ISGs with low expression values (below 10 reads) or expressed in less than 5% of tumors were excluded. The data were used for self-organizing map (SOM) clustering, which is an unsupervised machine learning approach enabling data dimensionality reduction without relying on any assumption about the data structure[41,42]. The SOM algorithm was iterated 100,000 times with Euclidean distance, linearly decreasing the learning rate from 0.05 to 0.01 using the R package Kohonen. The ISG expression patterns were projected onto a two-dimensional 10×10 hexagonal map. Thus, each node in this map is an expression profile representing a subset of the samples. SOM output, trained on the basis of 100,000 iterations, was used to estimate the contribution of each ISG to defining the clusters as a variance weighted according to the size of each node. A total of six clusters were estimated by the kmeans algorithm and

used to generate an expression heatmap. Expression *Z*-scores of the top 100 ISGs ranked on the basis of their contribution to defining the clusters were plotted using the R package pheatmap. Pearson correlation coefficients and corresponding FDR-adjusted *P* values were calculated between *Z*-scores for the top 100 ISGs and both *ACE2* and *dACE2* in cluster 5, which included 114 tumors with the highest ISG expression. The analysis was performed using the R package Hmisc.

In silico analysis of promoter regulatory elements relevant for IFN signaling. Promoters were defined within the −800 bp/+100 bp window from the corresponding TSSs. The window was limited by 800 bp, based on the intronic distance between the TSS of Ex1c and its upstream exon. Promoters of *ACE2*-Ex1a (P1), *ACE2*-Ex1b (P2) and *dACE2*-Ex1c (P3) were analyzed using Nsite tool[43] from the online bioinformatics gateway Softberry (http://www.softberry.com) to predict transcription-factor-binding sites. The search was set against the Object-oriented Transcription Factors Database of human and animal transcription-factor-binding sites largely curated according to the functional data from the literature. The parameters were set to allow a maximum of 1 or 2 mismatches with the known motifs. ISG-type motifs were manually curated from ~300 predicted and annotated motifs per promoter.

Luciferase promoter assays. *ACE2*-P1, *ACE2*-P2 and *dACE2*-P3 promoters (here defined as −800/−1 bp from the corresponding TSS), and two variants of the *dACE2*-P3 promoter with 100-bp deletions harboring predicted ISG-type motifs (Fig. 2b), were custom-synthesized by Thermo Fisher and cloned upstream of the luciferase reporter in a promoterless vector pGL4.21 (Promega) using the Xho1 and HindIII restriction sites. HepG2 cells were seeded in 96-well plates (4×10^3 cells per well) and 24 h after plating transiently co-transfected with the corresponding luciferase constructs together with a normalization control (*Renilla* pGL4.74 plasmid, Promega, in a 10:1 ratio), in six biological replicates per construct. The medium was changed 6 h after transfection and cells were treated with IFN-β (1 ng ml^{-1}, R&D Systems), IFN-γ (2 ng ml^{-1}, R&D Systems) or medium (mock) starting from 48 h post-transfection. After 6 h of treatment, cells were lysed and analyzed with the GloMax multi-detection system (Promega) and the luciferase levels in each well were normalized to the corresponding *Renilla* levels. The results were normalized by respective mock-treated controls and are presented as fold change over the negative control (empty pGL4.21 vector).

Mining of proteomics datasets. Mass spectrometry datasets generated for TCGA colon, breast and ovarian tumors (http://www.pepquery.org/) were mined for matches to the 36-aa fragment of dACE2, including the unique 10 aa encoded by *dACE2*-Ex1c. The analysis was performed with the PepQuery peptide-centric search engine[24], using the following parameters: mass spectrometry dataset of a specific cancer type; target event as protein; scoring algorithm as hyperscore and not selecting for unrestricted modification filtering. The identified peptides for each cancer type were exported as CSV files and manually analyzed for further assessment of peptide quality.

Transient transfections. Transient transfections were performed with Lipofectamine 3000 (Thermo Fisher). Unless specified, T24, a bladder cancer cell line in which no baseline expression of *ACE2* or *dACE2* was detected (Supplementary Table 2a), was used for transfections at 70–90% confluency in 12- or 6-well plates for 24 h.

Western blot. Cells were lysed with RIPA buffer (Sigma) supplemented with protease inhibitor cocktail (Promega) and PhosSTOP (Roche) and placed on ice for 30 min, with vortexing every 10 min. Lysates were pulse-sonicated for 30 s, with 10 s burst-cooling cycles, at 4°C, boiled in reducing sample buffer for 5 min and resolved on 4–12% Bis-Tris Bolt gels and transferred using an iBlot 2 (Thermo Fisher). Blots were blocked in 2.5% milk in 1% TBS–Tween before staining with antibodies (Supplementary Table 5). The signals were detected with HyGLO Quick Spray (Denville Scientific) or SuperSignal West Femto Maximum Sensitivity Substrate (Thermo Fisher) and viewed on a ChemiDoc Touch Imager with Image Lab 5.2 software (Bio-Rad).

Cell surface biotinylation and pulldown with streptavidin beads. T24 cells were transiently transfected with dACE2–Myc, ACE2–Myc or both constructs for 24 h. Cell surface biotinylation and pulldown with streptavidin beads were carried out using the Pierce Cell Surface Biotinylation and Isolation kit (Thermo Fisher). Briefly, the cell surface of T24 cells was biotinylated using EZ-Link sulfo-NHS-SS-biotin. Cells were lysed with RIPA buffer (Sigma) supplemented with protease inhibitor cocktail (Promega) and PhosSTOP (Roche) and placed on ice for 30 min, with vortexing every 10 min. Lysates were pulse-sonicated for 30 s, with 10 s burst-cooling cycles, at 4 °C. Biotinylated proteins were isolated with Neutravidin beads supplied with the kit. Input lysates and pulldown proteins from biotin$^+$ and biotin$^-$ fractions were analyzed by western blotting with the C-terminal ACE2 antibody (Abcam) as described above and anti-GAPDH antibody (Abcam).

Confocal microscopy. T24 cells were transiently transfected with ACE2–GFP or dACE2–Myc, or co-transfected with both constructs in 4-well chambered slides (2×10^4 cells per well, LabTek). After 24 h, cells were treated with 2 ng ml^{-1} of recombinant biotinylated SARS-CoV-2 spike protein RBD (spike protein RBD, Sino Biological) for 1 h at 37 °C. Cells were washed twice with medium and then stained with 5 μg ml^{-1} streptavidin PE (Thermo Fisher) for 30 min at 37 °C. Cells were then washed twice with PBS and fixed with 4% paraformaldehyde (BD Biosciences) for 30 min. After rinsing twice in PBS and permeabilization buffer (BD Biosciences), cells were incubated with permeabilization buffer for 1 h. Fixed cells were incubated with rabbit anti-FLAG antibody (1:250 dilution, Thermo Fisher) overnight, washed and then stained with anti-rabbit Alexa Fluor 680 (1:500 dilution, Thermo Fisher). Slides were mounted with antifade mounting media with DAPI (Thermo Fisher) and imaged at ×40 magnification on an LSM700 confocal laser scanning microscope (Carl Zeiss) using an inverted oil lens.

Flow cytometry analysis of SARS-CoV-2 spike protein RBD binding. T24 cells were transiently transfected with ACE2–GFP or dACE2–Myc, or co-transfected with both constructs in 12-well plates (1×10^4 cells per well). After 24 h, cells were stained with recombinant biotinylated spike protein RBD as described above and analyzed with multiparametric flow cytometry on a FACS Aria III (BD Biosciences) and FlowJo v10 software (BD Biosciences).

Carboxypeptidase activity assays. T24 cells were plated overnight in T-25 flasks (5×10^5 cells per flask) and transiently transfected with 10 μg of ACE2–GFP, dACE2–GFP or empty GFP vector. At 24 h post-transfection, cells were pelleted and lysed with 400 μl of the lysis buffer provided with the ACE2 activity kit (no. K897, BioVision). Keeping the reaction volumes and the amount of ACE2–GFP lysates constant, we added dACE2–GFP lysate in the ratio of 0.25, 0.5 and 1.0 to ACE2–GFP, with differences in volume compensated by lysates from GFP-expressing cells. The lysate mixtures were processed in triplicates using the kit reagents and according to the protocol. The carboxypeptidase activity was measured as fluorescence (Ex/Em = 365/410–460 nm) using a Promega GlowMax plate reader for two time points between 30 min and 2 h after adding the corresponding substrate mix. A positive control was provided by the kit. Cell lysates were also analyzed by western blots with C-terminal anti-ACE2 antibody (Abcam), which detects both ACE2 and dACE2, with GAPDH as a loading control.

Statistical analysis. Expression of *ACE2*-Ex1a, *ACE2*-Ex1b and *dACE2*-Ex1c between groups of samples was evaluated by two-sided tests: unpaired non-parametric Mann–Whitney *U* tests, paired Student's *t*-tests (for NHBE cells from five donors and organoids for three donors) and unpaired Student's *t*-tests (for biological replicates of cell lines and organoids from one donor). Statistical tests for other analyses are indicated in the corresponding sections. FDR adjustment was applied when indicated. *P* values < 0.05 were considered significant.

Computational resources. We used the NIH Biowulf supercomputing cluster and specific packages for R version 3.6.2.

Reporting Summary. Further information on research design is available in the Nature Research Reporting Summary linked to this article.

Data availability

The sequence for *dACE2* was deposited to NCBI GenBank with the accession number MT505392. The RNA-seq dataset of a breast cancer cell line, T47D, infected with SeV was deposited as NCBI SRA: PRJNA512015. The accession numbers for all of the data used in the paper are presented in Supplementary Table 6. Source data are provided with this paper. Requests for any additional data or reagents should be addressed to L.P.-O. (prokuninal@mail.nih.gov).

References

40. Prokunina-Olsson, L. et al. A variant upstream of *IFNL3* (*IL28B*) creating a new interferon gene *IFNL4* is associated with impaired clearance of hepatitis C virus. *Nat. Genet.* **45**, 164–171 (2013).
41. Nikkila, J. et al. Analysis and visualization of gene expression data using self-organizing maps. *Neural Netw.* **15**, 953–966 (2002).
42. Vesanto, J. & Alhoniemi, E. Clustering of the self-organizing map. *IEEE Trans. Neural Netw.* **11**, 586–600 (2000).
43. Shahmuradov, I. A. & Solovyev, V. V. Nsite, NsiteH and NsiteM computer tools for studying transcription regulatory elements. *Bioinformatics* **31**, 3544–3545 (2015).

Acknowledgements

We thank N. Cole (DCEG/NCI) for help with the acquisition of TCGA sliced BAM files and D. Proud (University of Calgary) for providing NHBE cells. We thank the CGR/DCEG/NCI for help with RNA-seq and authentication of cell lines by Identifiler profiling. The results are partially based on data generated by the TCGA Research Network. The project was supported by the Intramural Research Program of the DCEG/NCI; the NIH grant R21AG064479-01 and a Brain Health Research Institute Pilot Award from Kent State University (H.P.); S.B. and M.L.S. received financial support from the Deutsche Forschungsgemeinschaft: project numbers 240245660 (SFB1129) 415089553

(Heisenberg) and 272983813 (TRR179) to S.B. and project number 416072091 to M.L.S. D.M.S. and D.L.T. received financial support from the Li Ka Shing Institute of Virology.

Author contributions

O.O.O., A.R.B. and L.P.-O. conceived and designed the study. L.P.-O. supervised the study. O.O.O., A.R.B., M.L.S., D.M.S., S.B. and L.P.-O. designed the experiments. O.O.O., A.R.B., M.L.S., D.M.S., W.Y., A.O., J.M.V., T.J.R., C.K. and P.D. performed the experiments and analyzed the data. J.L.M. analyzed structural features of isoforms. A.R.B. performed computational analyses and quantification of RNA-seq datasets. A.R.B., O.O.O., H.P. and O.F.-V. performed statistical analyses. O.O.O., A.R.B., M.L.S., S.B., D.M.S., D.L.T. and L.P.-O. contributed reagents/materials/analysis tools. O.O.O., A.R.B. and L.P.-O. wrote the manuscript. All authors discussed the results and commented on the manuscript.

Competing interests

The authors declare no competing interests.

Additional information

Extended data is available for this paper at https://doi.org/10.1038/s41588-020-00731-9.

Supplementary information is available for this paper at https://doi.org/10.1038/s41588-020-00731-9.

Correspondence and requests for materials should be addressed to L.P.-O.

Peer review information *Nature Genetics* thanks David Levy, Carly Ziegler and the other, anonymous, reviewer(s) for their contribution to the peer review of this work. Peer reviewer reports are available.

Reprints and permissions information is available at www.nature.com/reprints.

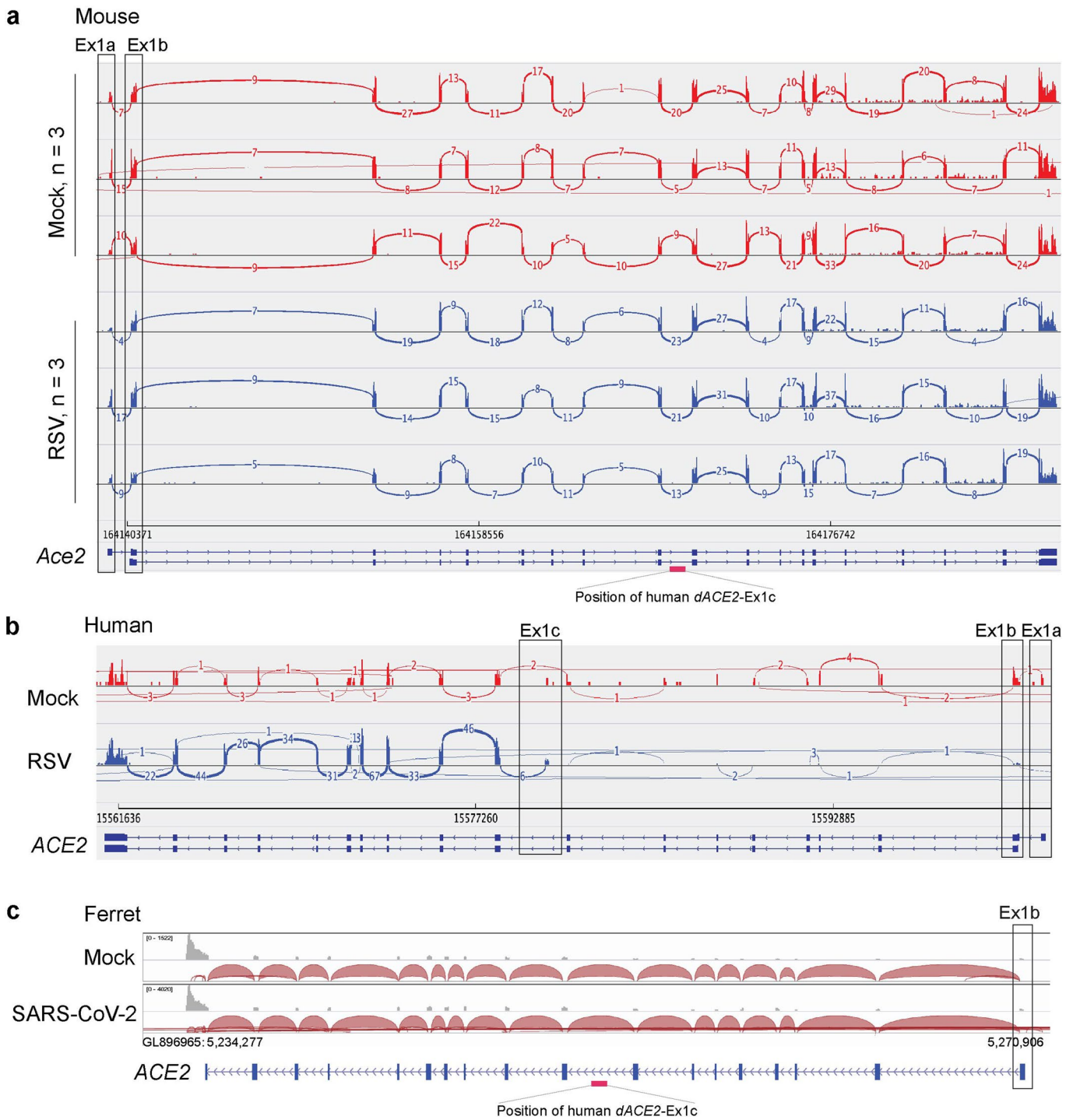

Extended Data Fig. 1 | *ACE2* expression patterns in the mouse and human lung cells infected with the respiratory syncytial virus (RSV) and nasal washes from ferrets infected with SARS-CoV-2. a, Sashimi plots of the *Ace2* region in a lung RNA-seq dataset from mice mock/RSV- infected in triplicates. The expression of *dAce2*-Ex1c is not observed and *Ace2* expression is not affected by the infection. **b**, Sashimi plots of the *ACE2* region in H292, a human lung mucoepidermoid pulmonary carcinoma cell line. Expression of *ACE2* from Ex1a and Ex1b is very low, while the *dACE2* from Ex1c is expressed at baseline and is further induced by RSV infection. **c**, Representative IGV plots showing exon and exon-exon junction RNA-seq reads from nasal washes of mock/SARS-CoV-2-infected ferrets. The expression of *dAce2*-Ex1c is not observed. Note: The mouse and human/ferret *ACE2/Ace2* genes are shown in opposite orientations, as presented in IGV. The positions corresponding to the human *dACE2*-Ex1c are marked in the mouse and ferret genomes. Datasets: PRJNA588982, PRJNA61503.

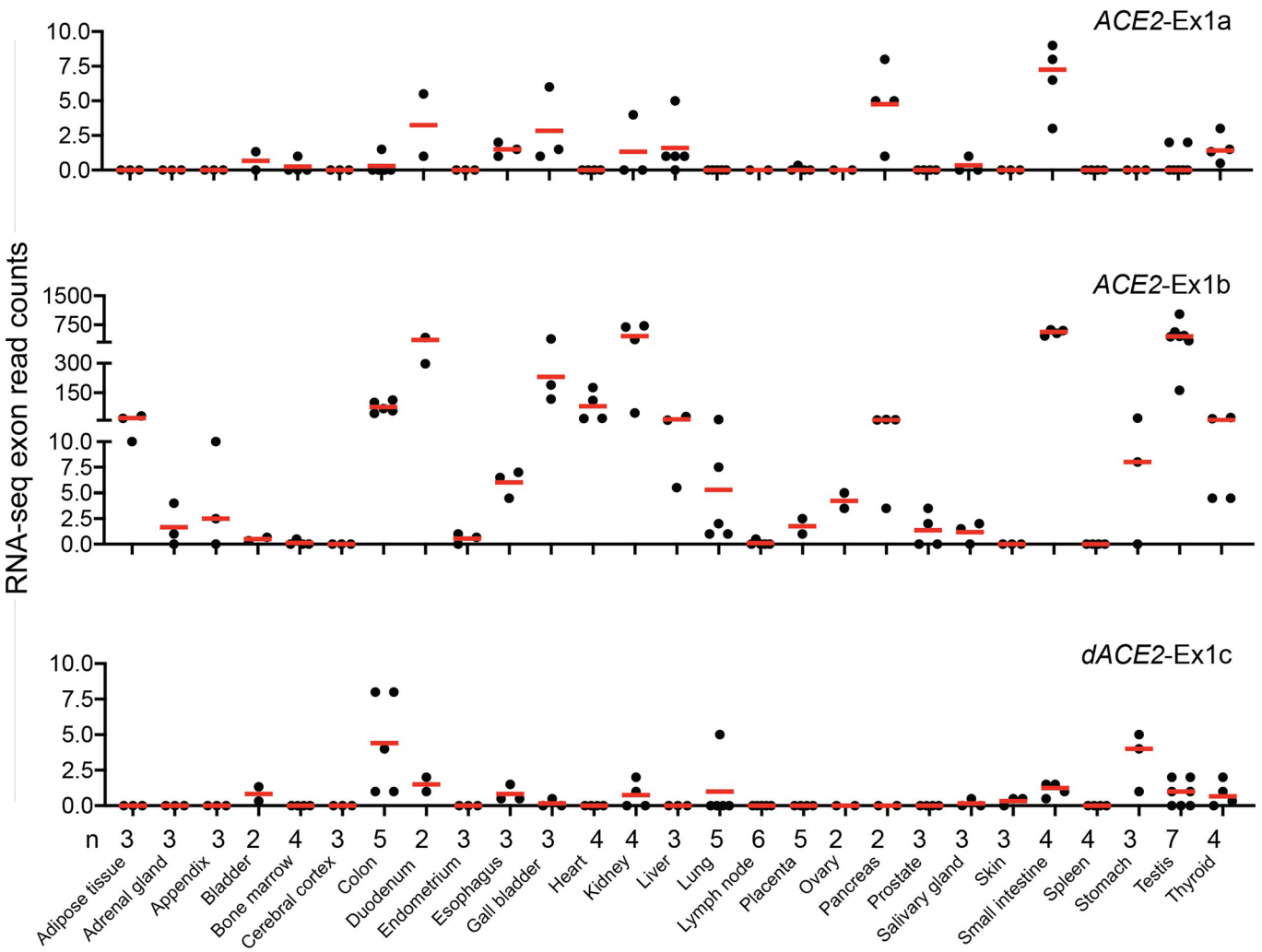

Extended Data Fig. 2 | *ACE2* and *dACE2* expression in normal human tissues. RNA-seq read counts for *ACE2*-Ex1a, *ACE2*-Ex1b, and *dACE2*-Ex1c in 27 human tissues. Dataset: PRJEB4337, n = 95.

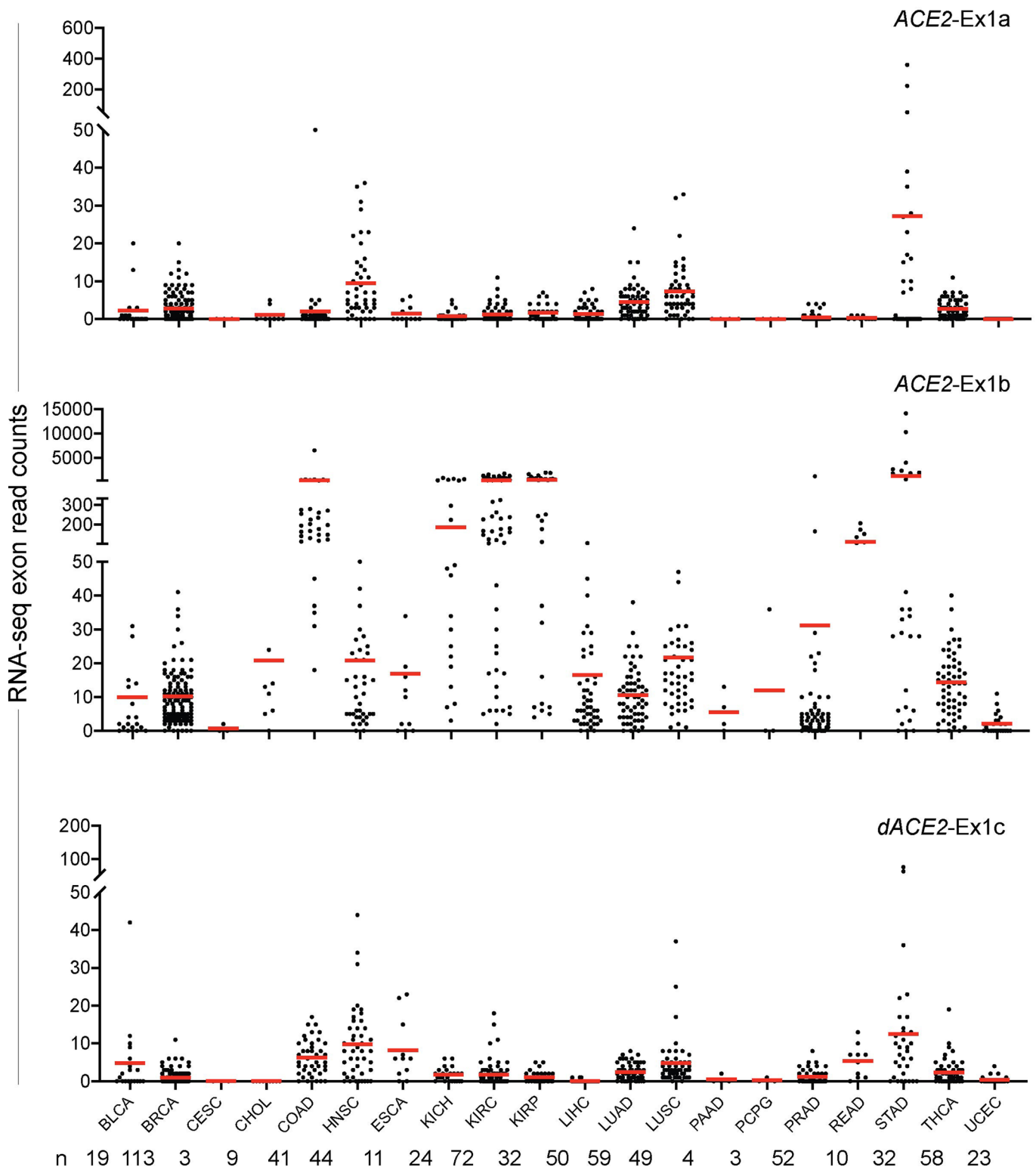

Extended Data Fig. 3 | *ACE2* and *dACE2* expression in tumor-adjacent normal tissues in TCGA. Based on RNA-seq read counts, *ACE2*-Ex1b is detectable in multiple samples of several tissue types. *dACE2*-Ex1c expression is more restricted and most common in normal tissue adjacent to tumors of head and neck (HNSC), stomach (STAD), lung squamous carcinoma (LUSC), colon (COAD), and esophagus (ESCA).

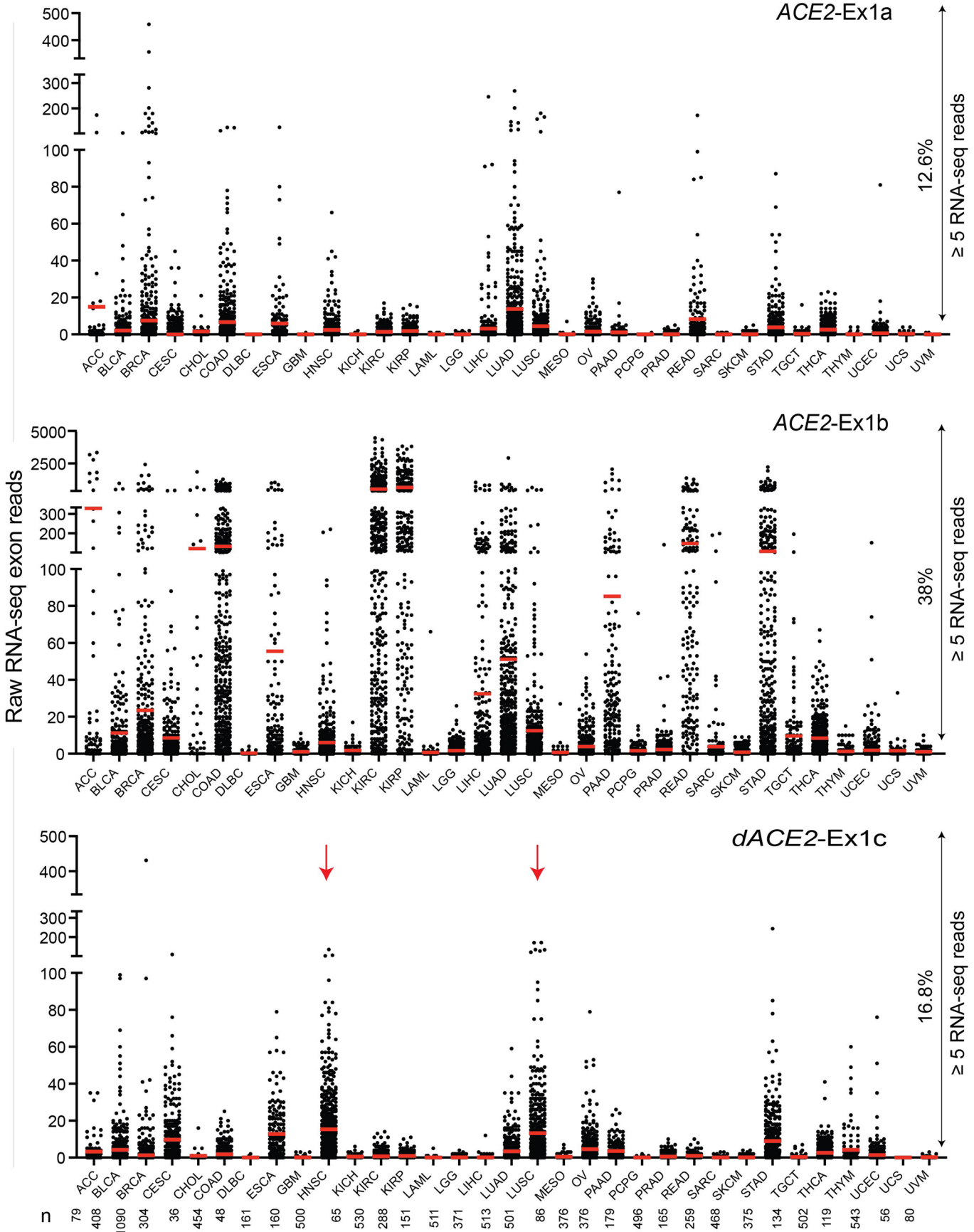

Extended Data Fig. 4 | See next page for caption.

Extended Data Fig. 4 | *ACE2* and *dACE2* expression across 10,185 tumors of 33 types in TCGA. Based on RNA-seq read counts, *ACE2*-Ex1b is most expressed in kidney tumors—kidney renal clear cell carcinoma (KIRC) and kidney renal papillary cell carcinoma (KIRP). Most samples expressing *dACE2*-Ex1c are squamous tumors of head and neck (HNSC) and the lungs (LUSC). Based on a ≥ 5 reads/sample threshold, *ACE2*-Ex1a is expressed in 12.6%, *ACE2*-Ex1b – in 38.0% and *dACE2*-Ex1c—in 16.8% of all tumors.

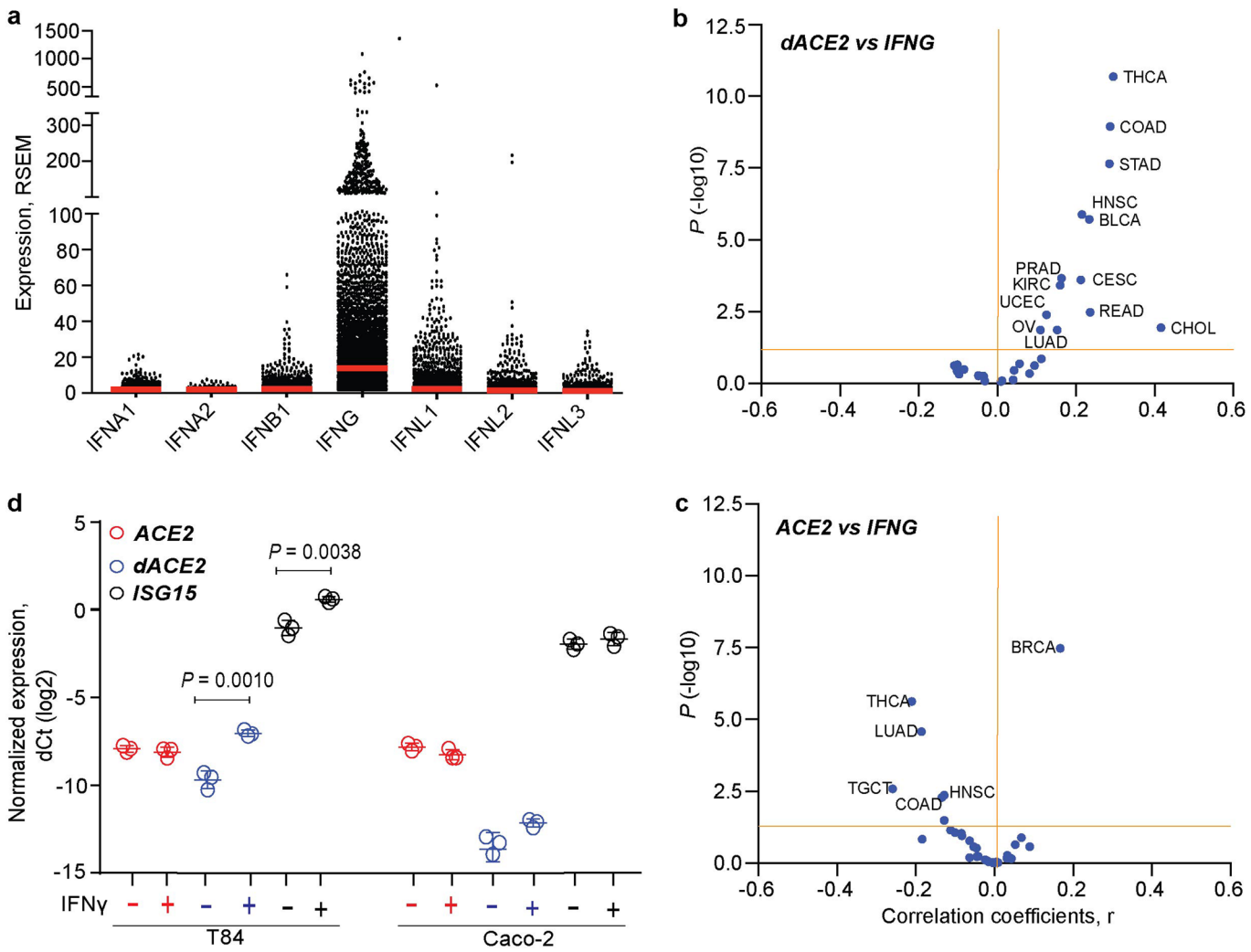

Extended Data Fig. 5 | *dACE2* and *ACE2* expression in relation to *IFNG* expression in TCGA tumors and in cells treated with IFNγ. a, Expression levels of all IFN genes annotated in TCGA tumors (n = 10,185) were acquired from cBioPortal (https://www.cbioportal.org/); expression of *IFNL4* was not annotated in this dataset. At RSEM ≥ 1, only expression of *IFNG* is common (61% samples), with mean RSEM = 19.8 compared to other IFN genes (mean RSEM ≤ 1.3). **b**, and **c**, Pearson correlation coefficients (r) for *dACE2* and *ACE2* vs. *IFNG* expression across tumors. *dACE2* showed significant positive correlations (r ≥ 0.2) with *IFNG* in 8 tumor types, while *ACE2* showed mainly negative correlations and only one positive correlation in breast cancer (r = 0.15). Expression values for *dACE2* and *ACE2* were based on log2-normalized exon read counts (Ex1b and Ex1c) and for *IFNG*—on RSEM values. **d**, Treatment of cell lines with IFNγ (2 ng/ml for 24 hrs) induced expression of *dACE2* but not *ACE2* in T84 cells. The results are presented with means +/- SD for three biological replicates; P-values are for the unpaired, two-sided Student's T-tests.

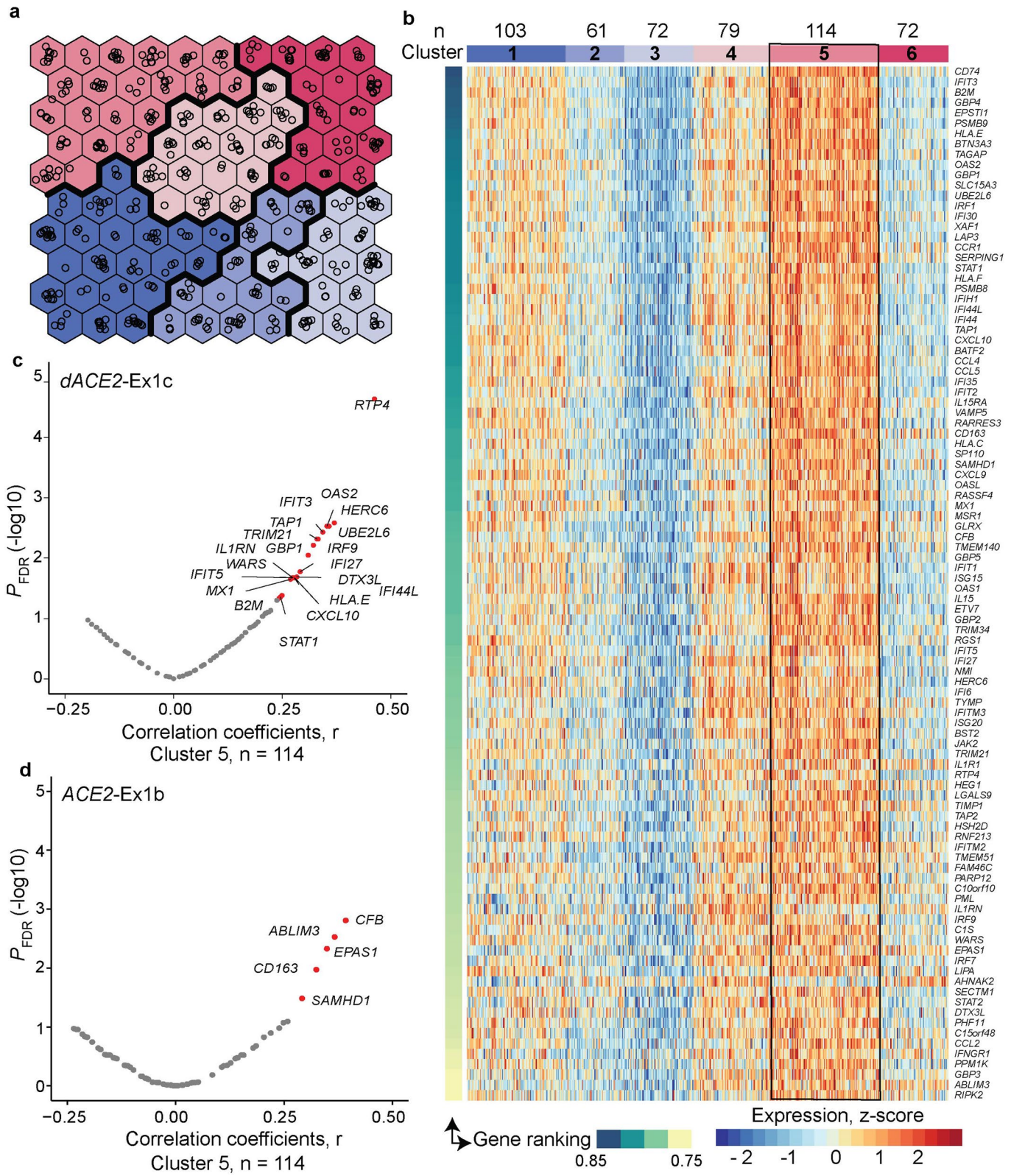

Extended Data Fig. 6 | Unsupervised self-organizing map (SOM) analysis in TCGA-LUSC tumors. a, Construction of the unsupervised SOM of TCGA-LUSC tumors (n = 501) based on Z-scores calculated for each of the 270 curated ISGs. Each hexagon includes a mean of 5 (range 1-14) tumors with similar ISG expression profiles. Colors denote clusters (1-6) of tumors with similar ISG expression profiles. **b**, Heatmap of the six SOM-defined clusters, visualized by plotting the expression levels of top 100 ISGs selected by the ranking of the initial set of 270 ISGs based on their contribution to these clusters. Cluster 5 includes 114 tumors with the highest ISG expression, whereas cluster 3 includes 72 tumors with the lowest ISG expression. **c**, and **d**, Volcano plots showing FDR-adjusted p-values and Pearson correlation coefficients (r), for two-sided tests, for expression of *dACE2* and *ACE2* in relation to the expression of the top 100 ISGs within cluster 5. In total, *dACE2* was significantly (FDR p-value < 0.05) correlated with the expression of 20 ISGs and *ACE2*—with 5 ISGs.

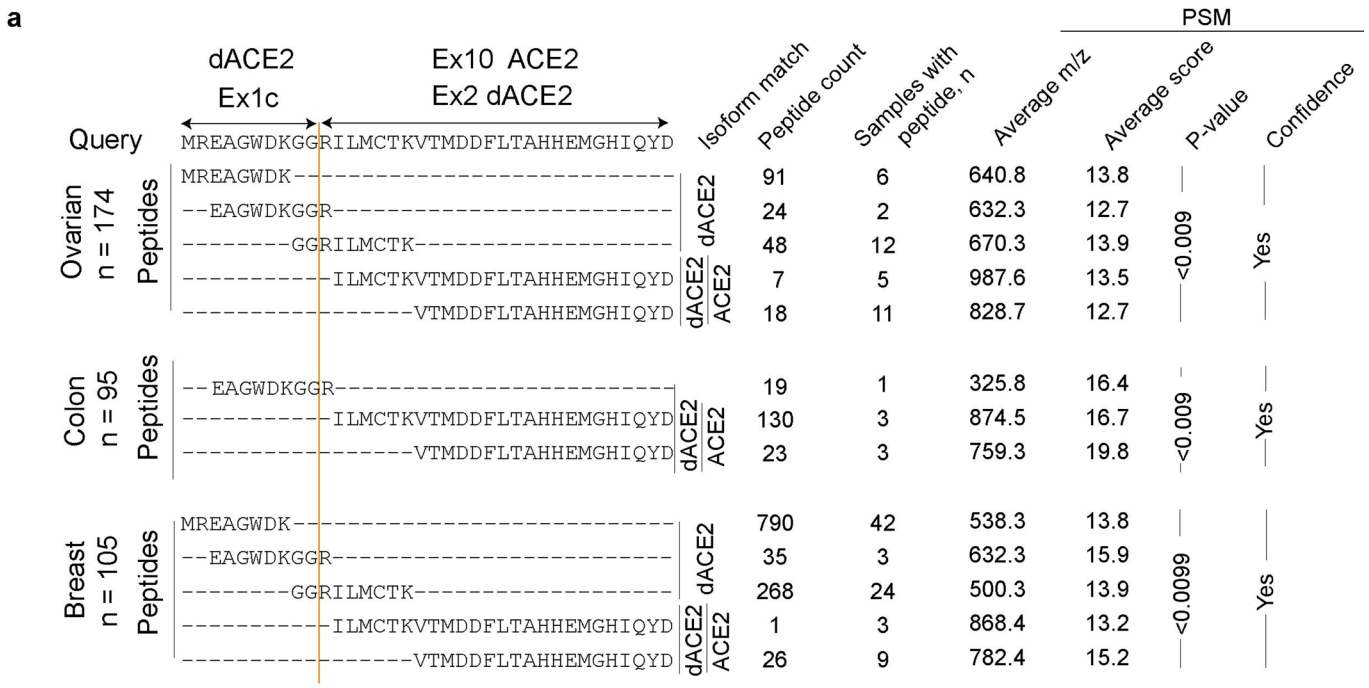

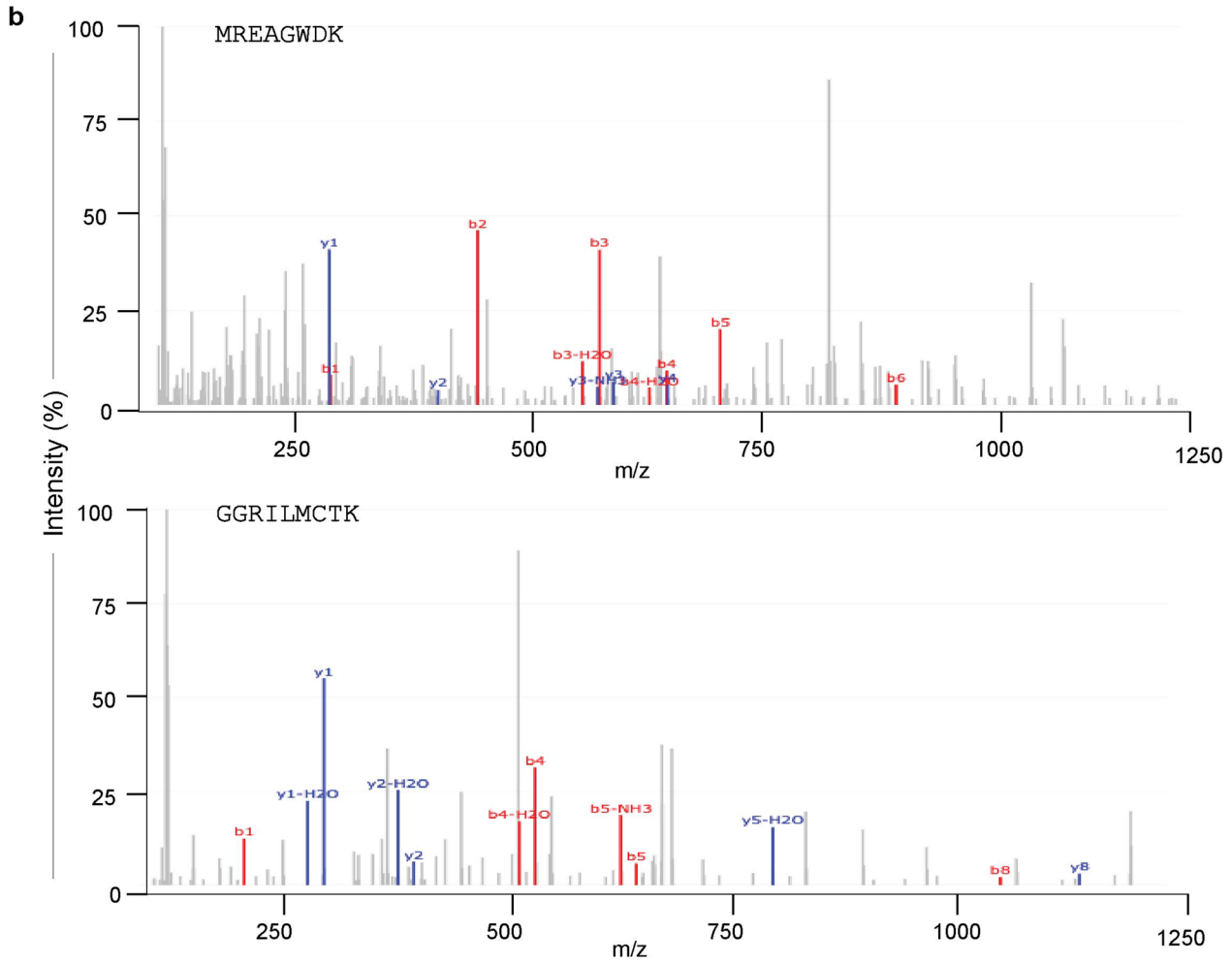

Extended Data Fig. 7 | See next page for caption.

Extended Data Fig. 7 | Peptides encoded by *dACE2*-Ex1c are detected by protein sequencing in tumors. a, Results of peptide query in PepQuery2 proteomics database of mass-spec data in 174 ovarian, 95 colon, and 105 breast tumors in TCGA[7]. Three peptides – MREAGWDK, EAGWDKGGR, and GGRILMCTK uniquely correspond to the 10 aa encoded by *dACE2*-Ex1c. The latter peptide results from the splicing of *dACE2*-Ex1c with its downstream exon. The total number of identified peptides, the number of samples with specific peptides, and corresponding parameters for a peptide-spectrum match (PSM) are shown in table format. **b**, Representative spectra of two peptides matching with the protein encoded by *dACE2*-Ex1c. M/z refers to the mass by charge ratio. The b-series and y-series ions showed the correct mapping of residues in the query aa sequence.

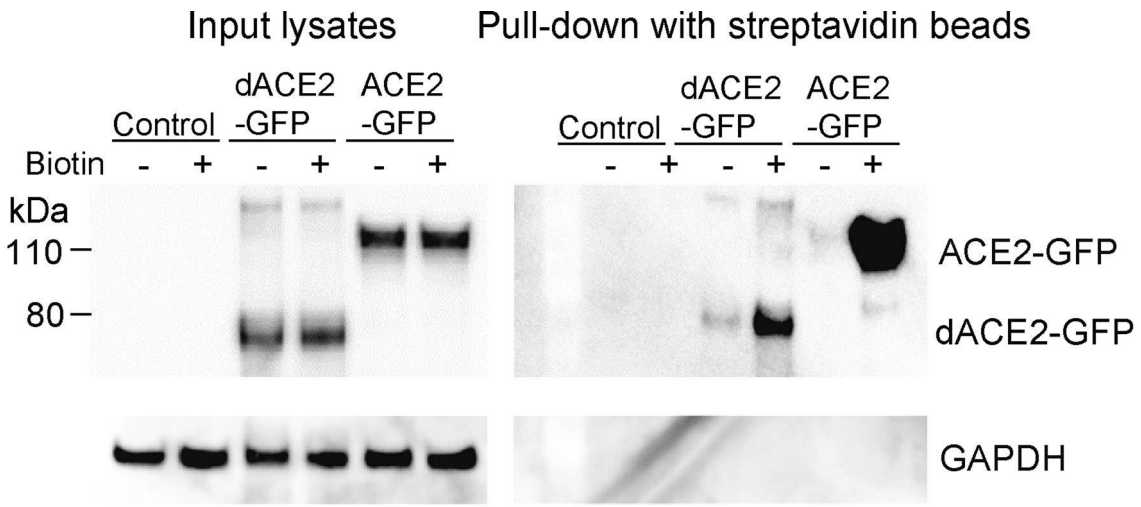

Extended Data Fig. 8 | Transiently overexpressed ACE2-GFP and dACE2-GFP are detectable on the cell surface. T24 cells were transiently transfected for 24 hrs with indicated constructs or not transfected (control) and then treated with (+) or without (-) biotin. Western blots with the C-terminal anti-ACE2 antibody detected a similar expression of both proteins in input lysates, but only in the biotin+ fraction after pull-down with streptavidin beads, showing much stronger expression of ACE2 compared to dACE2. GAPDH, a cytoplasmic protein, is undetectable in the pull-down fraction. The experiment was repeated three times, and representative results are shown.Source data

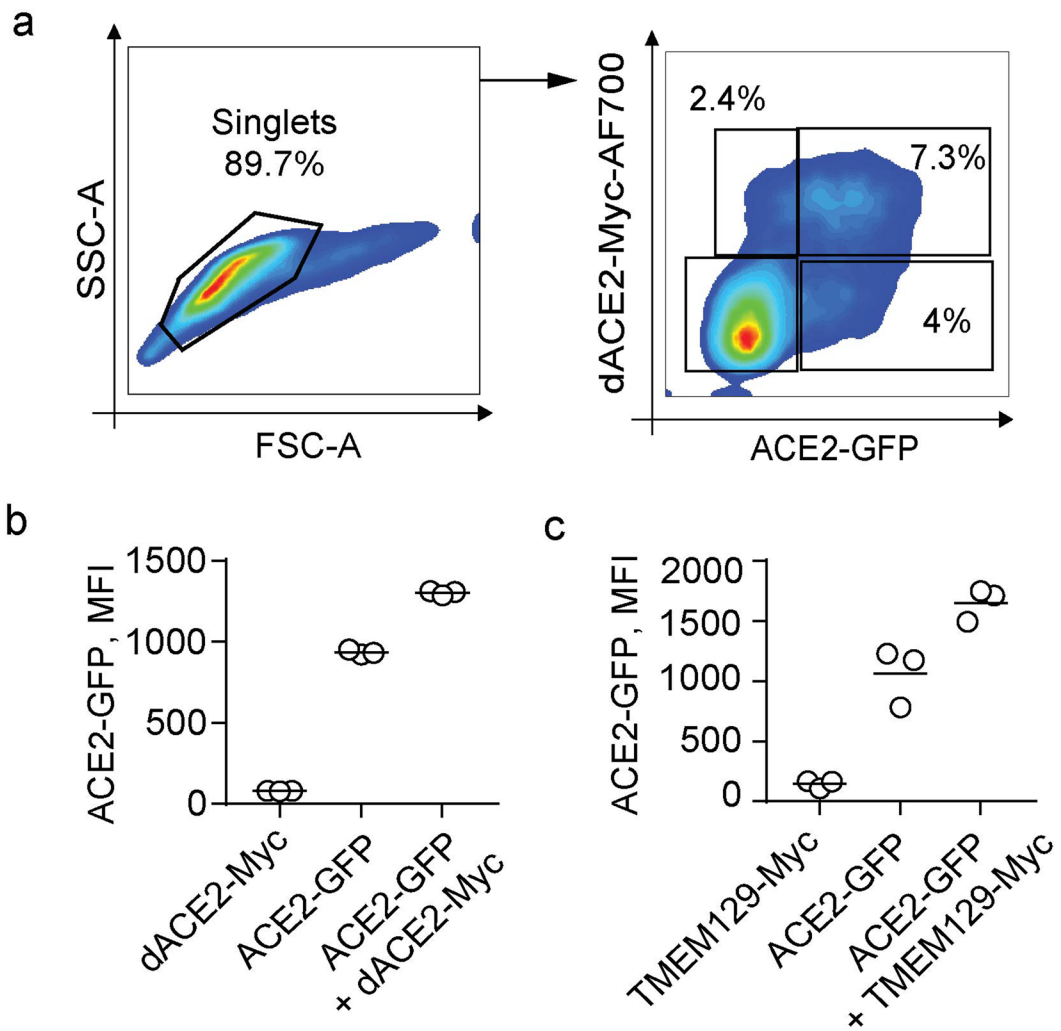

Extended Data Fig. 9 | ACE2-GFP levels are non-specifically increased in cells co-transfected with dACE2-Myc or TMEM129-Myc. a, A representative flow cytometry plot showing gates for the T24 cells co-transfected with dACE2-Myc and ACE2-GFP, corresponding to Fig. 7d, and **e**. The gates were drawn to identify cells expressing dACE2-Myc, ACE2-GFP, or both proteins. **b**, and **c**, Mean fluorescence intensity (MFI) of ACE2-GFP expression in the T24 cells transiently co-transfected in triplicates with ACE2-GFP and dACE2-Myc **b**, or ACE2-GFP and TMEM129-Myc **c**, and gated as described in **a**. TMEM129 is a transmembrane protein, which serves as an independent control, showing that the increase in ACE2-GFP expression might be a non-specific effect due to transfection rather than due to dACE2 co-expression.

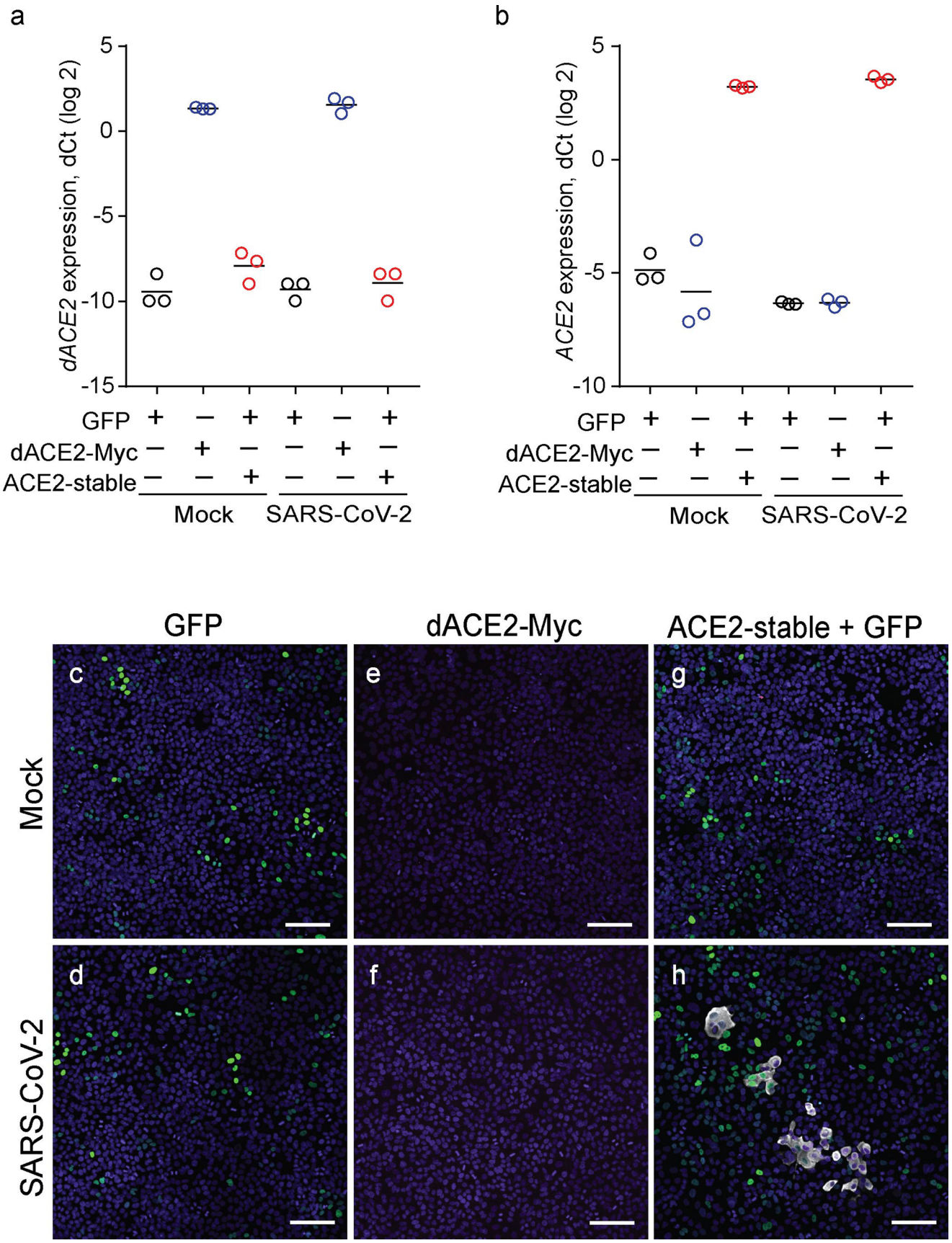

Extended Data Fig. 10 | See next page for caption.

Extended Data Fig. 10 | Immunofluorescence analysis of SARS-CoV-2 infection in the A549 cells. a, and **b**, Quantification of *dACE2* expression **a**, and *ACE2* expression. **b**, in SARS-CoV-2 (MOI = 1) or mock-infected lung cancer cell line A549 transfected with GFP (used as a transient transfection control), dACE2-Myc, or stably expressing ACE2 (ACE2-stable cell line) and transfected with GFP. The results are presented with means for three biological replicates. **c-h**) Immunofluorescence images in cells corresponding to plots **a**, and **b**. Cells were fixed and stained 72 hours after infection—SARS-CoV-2 nuclear protein (white), nuclei—DAPI (blue). Representative images from one of three biological replicates are shown. Corresponding plots for viral load and % of infected cells are presented in Fig. 7**f** and **g**. Scale bars, 100 μM.

nature research

Corresponding author(s): Prokunina-Olsson

Last updated by author(s): 09/22/2020

Reporting Summary

Nature Research wishes to improve the reproducibility of the work that we publish. This form provides structure for consistency and transparency in reporting. For further information on Nature Research policies, see our Editorial Policies and the Editorial Policy Checklist.

Statistics

For all statistical analyses, confirm that the following items are present in the figure legend, table legend, main text, or Methods section.

n/a	Confirmed
☐	☒ The exact sample size (*n*) for each experimental group/condition, given as a discrete number and unit of measurement
☐	☒ A statement on whether measurements were taken from distinct samples or whether the same sample was measured repeatedly
☐	☒ The statistical test(s) used AND whether they are one- or two-sided *Only common tests should be described solely by name; describe more complex techniques in the Methods section.*
☐	☒ A description of all covariates tested
☐	☒ A description of any assumptions or corrections, such as tests of normality and adjustment for multiple comparisons
☐	☒ A full description of the statistical parameters including central tendency (e.g. means) or other basic estimates (e.g. regression coefficient) AND variation (e.g. standard deviation) or associated estimates of uncertainty (e.g. confidence intervals)
☐	☒ For null hypothesis testing, the test statistic (e.g. *F*, *t*, *r*) with confidence intervals, effect sizes, degrees of freedom and *P* value noted *Give P values as exact values whenever suitable.*
☒	☐ For Bayesian analysis, information on the choice of priors and Markov chain Monte Carlo settings
☐	☒ For hierarchical and complex designs, identification of the appropriate level for tests and full reporting of outcomes
☐	☒ Estimates of effect sizes (e.g. Cohen's *d*, Pearson's *r*), indicating how they were calculated

Our web collection on statistics for biologists contains articles on many of the points above.

Software and code

Policy information about availability of computer code

Data collection	RNA-seq datasets listed in Table S7 were downloaded from NCBI SRA using SRA toolkit version 2.3.2. BAM files were generated with STAR version 7.1.3a by aligning to the GRChg38/hg38 genome assembly. Samples with less than 80% of mappable reads were excluded. BAM files were indexed and sliced using SAM tools to include 51.6 Kb of the ACE2 genomic region (chrX:15,556,393-15,608,016, hg38). For mouse RNA-seq data sets, the alignment was done with reference genome mm10 and and MusPutFur1.0 for ferret. For TCGA STAR-aligned RNA-seq data, BAM slices for the ACE2 region were acquired for 11, 041 TCGA samples (10,328 tumors and 713 tumor-adjacent normal tissues) through the NCI Genomics Data Commons (GDC) portal accessed on May 12, 2020, using workflow https://docs.gdc.cancer.gov/API/Users_Guide/BAM_Slicing/.
Data analysis	1. The FASTQ files were compressed using GZIP and aligned with STAR version 7.1.3a to the GRChg38/hg38 genome assembly. 2. Exon quantification from BAM files was performed using ASpli package (version 1.5.1: https://bioconductor.org/packages/release/bioc/vignettes/ASpli/inst/doc/ASpli.pdf) on R platform (versions 3.6.0 and above). 3. Integrative Genomics Viewer version 2.8.9 (http://www.broadinstitute.org/igv) was used for RNA-seq visualization 4. Clustal Omega version 2 (http://www.ebi.ac.uk/Tools/msa/clustalo/) for multiple sequence alignment of protein and nucleotide sequences 5. For identification of transcription factor binding motifs in promoters, we used: Nsite tool (version N/A) from online bioinformatics gateway Softberry (http://www.softberry.com/berry.phtml?topic=nsite&group=programs&subgroup=promoter). 6. Statistical analysis was performed using generic R tools version 3.6.2 and Prism - GraphPad (version 7)

For manuscripts utilizing custom algorithms or software that are central to the research but not yet described in published literature, software must be made available to editors and reviewers. We strongly encourage code deposition in a community repository (e.g. GitHub). See the Nature Research guidelines for submitting code & software for further information.

Data

Policy information about availability of data

All manuscripts must include a data availability statement. This statement should provide the following information, where applicable:

- Accession codes, unique identifiers, or web links for publicly available datasets
- A list of figures that have associated raw data
- A description of any restrictions on data availability

Only publicly available datasets were used in this analysis, all available from NCBI Short Read Archive (SRA) with accession numbers: PRJNA512015; PRJNA627860; PRJNA557257; PRJNA588982; PRJEB4337; PRJNA512015T and PRJNA615032. TCGA data was accessed on May 12, 2020 though NCI Genomics Data Commons (GDC). The quantification of ACE2 and dACE2 expression based on corresponding first exons Ex1b and Ex1c for the whole TCGA dataset (10,185 tumors and 713 tumor-adjacent normal tissue samples) was provided as Supplementary Table 3. Raw data for all expression assays in this study is provided as Table S2. The full-length sequence for human dACE2 derived by cloning and sequencing was deposited to NCBI GenBank (accession number MT505392), https://www.ncbi.nlm.nih.gov/nuccore/MT505392. TCGA proteomics data was accessed and analyzed with PepQuery database/tools (http://pepquery.org/). Nsite tool uses Object oriented Transcription Factors Database (ooTFD) accessible at https://www.hsls.pitt.edu/obrc/index.php?page=URL1100875281

Field-specific reporting

Please select the one below that is the best fit for your research. If you are not sure, read the appropriate sections before making your selection.

☒ Life sciences ☐ Behavioural & social sciences ☐ Ecological, evolutionary & environmental sciences

For a reference copy of the document with all sections, see nature.com/documents/nr-reporting-summary-flat.pdf

Life sciences study design

All studies must disclose on these points even when the disclosure is negative.

Sample size	Most of the data used in this analysis were acquired from public datasets The Cancer Genome Atlas (TCGA) and NCBI SRA. In TCGA - only duplicated samples were excluded. The RNA-seq data from TCGA tumors includes 10,185 samples which is sufficient for analyzing expression of ACE2 isoforms. For other datasets - only samples with at least 80% of mappable reads were analyzed.
Data exclusions	Except duplicates no samples were excluded from the analysis.
Replication	Yes, all experimental findings were reliably reproduced in multiple biological and technical replicates. Results were verified with minimum of three independent experiments.
Randomization	Not applicable
Blinding	All samples were processed blindly to their phenotype status

Reporting for specific materials, systems and methods

We require information from authors about some types of materials, experimental systems and methods used in many studies. Here, indicate whether each material, system or method listed is relevant to your study. If you are not sure if a list item applies to your research, read the appropriate section before selecting a response.

Materials & experimental systems

n/a	Involved in the study
☐	☒ Antibodies
☐	☒ Eukaryotic cell lines
☒	☐ Palaeontology and archaeology
☒	☐ Animals and other organisms
☐	☒ Human research participants
☒	☐ Clinical data
☒	☐ Dual use research of concern

Methods

n/a	Involved in the study
☒	☐ ChIP-seq
☐	☒ Flow cytometry
☒	☐ MRI-based neuroimaging

Antibodies

Antibodies used

Target gene | Cat. No. | Source | Target species | Host | Tag | Dilution
1. ACE2 ab15348 Abcam Human Rabbit 1:250 Lot: GR333640-15
2. Myc-DDK F7425 Sigma Tag Rabbit 1:1000 Lot: 078M4886V
3. GAPDH Ab9485 Abcam Human Rabbit 1:1000 Lot: GR3309101-1
4. GFP MA515256 Thermo Fisher Tag Mouse 1:1000 Lot: UJ284110

5. IgG #7074 Cell Signaling Rabbit Goat HRP 1:5000 Lot 28
6. IgG sc2314 Santa Cruz Mouse Donkey HRP 1:5000 Lot: D0108
7. IgG sc2304 Santa Cruz Goat Donkey HRP 1:5000 Lot: A0408
8. Streptavidin SA10044 Thermo Fisher Tag PE 1:200 Lot: 2147622
9. IgG A10038 Thermo Fisher Rabbit Donkey AF680 1:200 Lot: 400467
10. SARS-CoV-2 NP 40143-MM05 Sino biologicals Viral Mouse 1:1000 Lot: LC14MA1902

Validation

Positive and negative controls were included in all the assays: Western blot and other specific applications.
1. ACE2 ab15348 Abcam Human Rabbit. Validated in WB, IHC and tested in Mouse, Rat, Cat, Human, Ferret, Macaque monkey. Cited in 21 publication(s).
2. Myc-DDK F7425 Sigma Tag Rabbit. The antibody recognizes the FLAG epitope located on FLAG-tagged fusion proteins at the N- or C-terminus, applying dot blot, immunoblotting, immunoprecipitation and immunocytochemistry assays.
3. GAPDH Ab9485 Abcam Human Rabbit. Loading Control. Validated in WB, IHC, ICC/IF and tested in Rat, Chicken, Human, Saccharomyces cerevisiae, Xenopus laevis
4. GFP MA515256 Thermo Fisher Tag Mouse. MA5-15256 recognizes native and denatured forms of GFP (Green Fluorescent Protein) and its many variants: EGFP, YFP, EYFP, and CFP. MA5-15256 has successfully been used in immunoprecipitation, ELISA, Western blotting, and immunofluorescence applications.

Eukaryotic cell lines

Policy information about cell lines

Cell line source(s)

Most of the cell lines used were purchased from the American Type Culture
Collection (ATCC). Other sources were CELLnTEC and International Institute for the Advancement of Medicine. Detailed information is provided in Table S4.

Authentication

Cells lines were freshly purchased from ATCC or if used longer than 6 months, authenticated by genotyping of a panel of microsatellite markers - Identifiler, performed by the Cancer Genomics Research Laboratory, NCI
Cells Source
Primary tonsil epithelial cells ScienCell Used within 6 months of purchase
T24 ATCC Used within 6 months of purchase
HT-1376 ATCC STR profiling
HTB-9 ATCC STR profiling
RT-4 ATCC STR profiling
TCCSUP/HTB5 ATCC STR profiling
5637/HTB9 ATCC STR profiling
J82 ATCC STR profiling
SW780 ATCC STR profiling
UMUC3 ATCC STR profiling
HBLAK CELLnTEC Used within 6 months of purchase
T47D (MDA-MB-23) ATCC STR profiling
HeLa ATCC STR profiling
Caco-2 ATCC Used within 6 months of purchase
T84 ATCC Used within 6 months of purchase
HepG2 ATCC STR profiling
293T ATCC STR profiling
A549 ATCC STR profiling
ACE2-A549 stable Gift from Ralf Bartenschlager STR profiling
Calu3 ATCC Used within 6 months of purchase
Capan-1 ATCC STR profiling
PC3 ATCC STR profiling
22RV1 ATCC STR profiling
DU145 ATCC STR profiling
NHBE International Institute for the Advancement of Medicine Used within 6 months of purchase

Organoid cultures of colon and ileum University Hospital Heidelberg Used within 6 months after generation from primary tissues

Mycoplasma contamination

All cell lines in the laboratory are regularly tested for mycoplasma contamination
using the MycoAlert Mycoplasma Detection kit (Lonza). Cell lines tested negative when compared to positive control

Commonly misidentified lines
(See ICLAC register)

No commonly misidentified cell lines were used.

Human research participants

Policy information about studies involving human research participants

Population characteristics

Describe the covariate-relevant population characteristics of the human research participants (e.g. age, gender, genotypic information, past and current diagnosis and treatment categories). If you filled out the behavioural & social sciences study design questions and have nothing to add here, write "See above."

Recruitment	*Describe how participants were recruited. Outline any potential self-selection bias or other biases that may be present and how these are likely to impact results.*
Ethics oversight	*Identify the organization(s) that approved the study protocol.*

Note that full information on the approval of the study protocol must also be provided in the manuscript.

Flow Cytometry

Plots

Confirm that:

☒ The axis labels state the marker and fluorochrome used (e.g. CD4-FITC).

☒ The axis scales are clearly visible. Include numbers along axes only for bottom left plot of group (a 'group' is an analysis of identical markers).

☒ All plots are contour plots with outliers or pseudocolor plots.

☒ A numerical value for number of cells or percentage (with statistics) is provided.

Methodology

Sample preparation	T24 cells were transiently transfected with ACE2-GFP, dACE2-Myc-DDK, or co-transfected with both constructs in 12-well plates (1x105 cells/well). After 24 hrs, cells were stained with recombinant biotinylated spike protein RBD. Similarly, Lung cancer cells A549 (wild-type or stably overexpressing human ACE2 (ACE2-stable)) were seeded either in 48-well plates (for RNA) or on iBIDI glass-bottom 8-well chamber slides (for immunofluorescence analysis) at a density of 7.5x104 cells/well or chamber. Cells were transduced 24 hrs post-seeding with lentiviruses expressing GFP or dACE2-Myc and infected 3 days post-transduction. Culture media was removed and the virus was added to cells for 1 hr at 37°C. After virus removal, cells were washed 1x with PBS, and media was added back to the cells. Cells were harvested 24 hrs post-infection for RNA extraction or were fixed in 4% paraformaldehyde (PFA) for 20 mins at room temperature (RT) for infectivity analysis by immunofluorescence staining, as was previously described.
Instrument	FACS Aria III (BD Biosciences)
Software	FlowJo.v10 software (BD Biosciences)
Cell population abundance	20,000 cells were analyzed per sample
Gating strategy	Singlet gate was generated using FSC-A vs FSA-H, cells were then analyzed comparing PE vs FITC channel

☒ Tick this box to confirm that a figure exemplifying the gating strategy is provided in the Supplementary Information.